Received: 9 June 2022 | Revised: 26 October 2022 | Accepted: 9 December 2022

DOI: 10.1002/glia.24325

GLIA

WILEY

RESEARCH ARTICLE

Human myeloid progenitor glucocorticoid receptor activation causes genomic instability, type 1 IFN- response pathway activation and senescence in differentiated microglia; an early life stress model

Jingzhang Wei[1] | Charles Arber[2] | Selina Wray[2] | John Hardy[2] | Thomas M. Piers[1] | Jennifer M. Pocock[1]

[1]Department of Neuroinflammation, University College London Institute of Neurology, London, UK

[2]Department of Molecular Neuroscience, University College London Institute of Neurology, London, UK

Correspondence
Jennifer M. Pocock and Thomas M. Piers, Department of Neuroinflammation, University College London Institute of Neurology, 1 Wakefield Street, London WC1N 1PJ, UK.
Email: j.pocock@ucl.ac.uk; t.piers@exeter.ac.uk

Present address
Thomas M. Piers, Living System Institute, Bioscience, University of Exeter, Exeter, UK.

Funding information
Alzheimer's Society UK, Grant/Award Number: AS-JF-18-008; Alzheimer's Research UK, Grant/Award Number: ARUK- SRF2016B-2; National Institute for Health Research; University College London Hospitals Biomedical Research Centre

Abstract

One form of early life stress, prenatal exposure to glucocorticoids (GCs), confers a higher risk of psychiatric and neurodevelopmental disorders in later life. Increasingly, the importance of microglia in these disorders is recognized. Studies on GCs exposure during microglial development have been limited, and there are few, if any, human studies. We established an in vitro model of ELS by continuous pre-exposure of human iPS-microglia to GCs during primitive hematopoiesis (the critical stage of iPS-microglial differentiation) and then examined how this exposure affected the microglial phenotype as they differentiated and matured to microglia, using RNA-seq analyses and functional assays. The iPS-microglia predominantly expressed glucocorticoid receptors over mineralocorticoid receptors, and in particular, the GR-α splice variant. Chronic GCs exposure during primitive hematopoiesis was able to recapitulate in vivo ELS effects. Thus, pre-exposure to prolonged GCs resulted in increased type I interferon signaling, the presence of Cyclic GMP-AMP synthase-positive (cGAS) micronuclei, cellular senescence and reduced proliferation in the matured iPS-microglia. The findings from this in vitro ELS model have ramifications for the responses of microglia in the pathogenesis of GC- mediated ELS-associated disorders such as schizophrenia, attention-deficit hyperactivity disorder and autism spectrum disorder.

Abbreviations: ADHD, attention-deficit hyperactivity disorder; ASD, autism spectrum disorder; cGAS, Cyclic GMP-AMP synthase; cor, correlation; Cort, hydrocortisone; CRH-expressing PVN neurons, corticotropin-releasing factor-containing neurons in the paraventricular nucleus; DEG, differentially expressed gene; Dex, dexamethasone; ELS, early life stress; FBS, fetal bovine serum; GC, glucocorticoids; GR, glucocorticoid receptors; GS, gene significance; GSEA, Gene set enrichment analysis; h, hr, hours; hMg, human microglia; HPA, hypothalamus pituitary adrenal; IFN, interferon; iPS- MPro, iPSC-derived myeloid progenitor; iPS-Mg, human induced pluripotent stem cell derived microglia; ISG, interferon-stimulated genes; min, minutes; MM, module membership; MR, mineralocorticoid receptor; MS, module significance; NR3C1, Nuclear Receptor Subfamily 3 Group C Member 1, gene name for glucocorticoid receptor; NT, non-treated; RU, RU486 GR antagonist; SASP, senescence-associated secretory phenotype; SA-β-gal, senescence-associated beta galactosidase; TOM, topological overlap matrix; TREM2, triggering receptor expressed on myeloid cells 2; WGCNA, weighted gene co-expression network analysis; wk, week.

KEYWORDS
cellular senescence, early life stress, genomic instability, glucocorticoid receptor, glucocorticoids, induced pluripotent stem cells, microglia, micronuclei

1 | INTRODUCTION

Psychosocial and physical stress activates the hypothalamic pituitary adrenal (HPA) axis, which produces glucocorticoids (GC) (Smith & Vale, 2006). GC are steroid hormones essential for maintaining biological rhythms and responding to stress; and are used exogenously to treat inflammation, autoimmune diseases, and cancer (Timmermans et al., 2019). Prolonged and excessive exogenous GC therapy and endogenous GC secretion are linked to cardiovascular disease (Faresjö et al., 2020), diabetes, and depression (Joseph & Golden, 2017). Chronic and dysregulated GC does not only occur in adult life but also early life.

Early life stress (ELS) is defined as an adverse environment or experience that an individual encounters in critical developmental periods. Estimated 65% of people in United States have experienced at least one adverse early life event, 12.5% have experienced as many as four (Middlebrooks & Audage, 2008). ELS, such as prenatal/maternal stress, has been significantly associated with increased risk of neurodevelopmental and psychiatric disorders later in life (Lupien et al., 2009; Manzari et al., 2019). One molecular mediator of ELS is prolonged elevated maternal GC during pregnancy and early life development (Krontira et al., 2020), and thus in utero chronic activation of its cognate receptors, glucocorticoid receptors (GR). Cortisol of maternal origin represents the primary source of cortisol in early gestation of the feotus (Harris & Seckl, 2011). Dysregulated maternal GCs/GR signaling increases fetal GC exposure (Benediktsson et al., 1993; Chen et al., 2021; Quinn et al., 2019; Swanson & David, 2015).

In vivo and human research have examined the link between dysregulated maternal GC and later-life illnesses. Rodent offspring exposed prenatally to high maternal GC had dysregulated HPA axis activity and aberrant stress reactivity (Barbazanges et al., 1996). Prenatal stress, such as restraint stress to rodent dams for 30 or 240 min from embryonic day 15 to 17, affects corticotropin-releasing factor-containing neurons in the paraventricular nucleus (CRH-expressing PVN neurons) of the hypothalamus (one component of HPA axis) in fetal brains (Fujioka et al., 1999). Fujioka et al. (1999) found that 30-min restrain stress caused more cell differentiation, but 240-min led to more apoptotic cells and shorter processes in CRH-expressing PVN neurons. Chronic prenatal stress from days 14–21 caused degeneration and apoptosis of CRH-expressing PVN neurons in male offspring (Baquedano et al., 2011). Fukumoto et al. (2009) found that synthetic GC exposure in pregnant rats impacted fetal neurodevelopment by inhibiting radial migration of cortical neurons during medial cortex development. Prenatal GC exposure to mother from gestational days 16 to 18 causes altered microglial function, schizophrenia-like behavior in male offspring mice, and depressive-like behavior in female offspring mice (Rim et al., 2022).

Human new-borns exposed to sGC in the second and third trimesters exhibit increased cortisol responses (Davis et al., 2011). Further research showed that higher maternal cortisol levels during early pregnancy (15 wk gestation) relate to structural alterations in the right amygdala and emotional difficulties in female offspring at age 7 (Buss et al., 2012). Children exposed to sGC during pregnancy had a greater risk of mental and behavioral disorders regardless of preterm or full-term (Wolford et al., 2020). Prenatal exposure to maternal sGC at 28.2 wk resulted to fewer neurons in neonates' hippocampus than without sGC (Tijsseling et al., 2012). Children exposed to sGC in utero exhibited thinner cortices, especially in the stress- and emotion-regulating rostral anterior cingulate cortex. These changes correlate with emotional issues in youngsters (Davis et al., 2013). Supporting evidence from neuroimaging studies relate prenatal sGC exposure to brain structural changes (Davis et al., 2011; Moog et al., 2018). Altogether, research reveal maternal GC and sGC during pregnancy have a deleterious influence on neurodevelopment and consequent mental and behavioral issues in children, and a few studies listed here suggest this effect is duration- and trimester-dependent.

In vitro model of prenatal stress by treating neuronal precursor cells derived from human-induced pluripotent stem cells (iPSC) with sGC (Dexamethasone, Dex) impairs the neuronal differentiation (Nürnberg et al., 2018). Exposing a human fetal hippocampus progenitor cell line to Dex during proliferation and neuronal differentiation leads to long-lasting DNA methylation alteration in genetic networks involved in axonal development, actin filament organization, cellular proliferation, and neurotransmission (Provençal et al., 2020). Provençal et al. (2020) found that long-lasting differentially methylated regions are linked with an increased transcriptional response to a second acute sGC exposure. Moreover, human iPS-derived astrocytes from depressive patients respond uniquely to both chronic and acute cortisol treatment (Heard et al., 2021). However, the effects of excessive GCs or GR stimulation have yet to be studied in relation to human microglial development and any subsequent microglial phenotypic changes.

Microglia are the primary immunocompetent cells within the central nervous system (CNS). During pre- and post-natal neurodevelopment, microglia participate in many neurodevelopmental processes, such as cortical neurogenesis (Cunningham et al., 2013; Schafer et al., 2012; Squarzoni et al., 2014; Weinhard et al., 2018), controlling migration of inhibitory neocortical interneurons that regulate excitation-inhibition balance (Squarzoni et al., 2014), and remodeling of synaptic structures (Schafer et al., 2012; Weinhard et al., 2018). Mounting evidence points to the involvement of microglia in psychiatric and neurodevelopmental disorders, including, schizophrenia (Mondelli et al., 2017), autism spectrum disorder and attention-deficit hyperactivity disorder (ADHD) (Courchesne et al., 2020).

Microglial development occurs in early embryonic life. Microglia are derived from the embryonic yolk sac, and first appear in the CNS around gestational week 4.5 in humans (Monier et al., 2007), and embryonic day 9.5 in mice (Ginhoux et al., 2010). In rat models, prenatal elevated GC was found to increase the overall density and immunoreactivity of embryonic microglia (Bittle & Stevens, 2018). Furthermore, aberrant GR activation, the cognate GC receptor, in early postnatal primary microglia reduces CX3CR1 and TREM2 expression and induced cellular senescence in early postnatal primary microglia (Park et al., 2019).

Therefore, we hypothesize that increased GC levels caused by prenatal GC overexposure could influence early microglial development and subsequent microglial phenotypes. Our study used human iPSC-derived microglia (iPS-Mg) from iPSC lines from people with distinct genetic backgrounds to construct an in vitro model of ELS. We report here that excessive GC at the stage of primitive hematopoiesis during microglial differentiation, resulted in increased interferon-alpha signaling, frequent formation of cGAS (a positive marker for micronuclei, Miller et al., 2021), positive micronuclei indicating possible genomic instability, and senescence-like features in differentiated iPS-Mg.

2 | MATERIALS AND METHODS

2.1 | Cell culture

2.1.1 | iPSC-derived microglia and treatment

This study was covered by ethics reference 09/H0716/64, from the National Hospital for Neurology and Neurosurgery and the Institute of Neurology's joint research ethics committee. A material transfer.

Disease Research Center enabled the acquisition of R47H heterozygous ($R47H^{het}$) patient-derived fibroblasts (UCI ADRC; Professor M Blurton-Jones) which we previously derived into iPSCs (Piers et al., 2020). The following lines and clones were used 26.5, 26.15, and 8.6 of the $R47H^{het}$ iPSC. In addition, the following lines from normal individuals expressing common variant TREM2 used in this study were SFC840 (Stembancc), BIONi010-C (EBiSC) and KOLF2_C1 (kindly provided by the Sanger Institute).

Using our previously described protocol, iPS-microglia (iPS-Mg) were generated (Cosker et al., 2021; Garcia-Reitboeck et al., 2018; Piers et al., 2020; Xiang et al., 2018). All iPSCs were cultured and passaged routinely in Essential 8 medium (Gibco), iPS-myeloid progenitor cells (iPS-MPro) were harvested from the flask of embryoid bodies and further differentiated with IL-34, MCSF and TGF-β1 for 14 days, plus a final maturation with CX3CL1 and CD200 (all growth factors were from Peprotech, London, UK) for 3 more days as previously described (Mallach et al., 2021; Piers et al., 2020).

To model ELS, 50 nM Dex (Tocris Bioscience, Abingdon, UK) or 500 nM hydrocortisone (Cort; Tocris Bioscience, Abingdon, UK) was added during the second stage of primitive hematopoiesis, which typically occur 2 weeks after the stem cell plating, when the embryoid bodies were first seeded into flasks, and subsequently at every week for approximately 12 weeks thereafter (Figure 1a) when the medium was replenished. These cells are referred to as iPS-myeloid progenitors (iPS-MPro). To block GR activation, 6 nM RU486 (Cayman, CAS#84371-65-3) was added 30 min before 50 nM Dex. This GR antagonistic paradigm has been used in other in vitro studies (Guess et al., 2010; Liu et al., 2017). The concentration of 6 nM of RU486 is based on the IC_{50} of RU486 (Attardi et al., 2004). Thus, throughout the rest of this article, Dex-iPS-Mg means that at the iPS-MPro stage, the cells were treated with Dex, and Cort-iPS-Mg means that at the iPS-MPro stage, cells were treated with Cort, and RU/Dex iPS-Mg (RU486 and Dex treated iPS-Mg) means that at the iPS-MPro stage, cells were treated Ru and Dex. NT-iPS-Mg means the cells at the iPS-MPro stage were not treated.

2.1.2 | Other cell lines

HeLa cells, kindly provided by Dr Jan Attig (The Crick Institute, London, UK), were maintained in Dulbecco's Modified Eagle's Medium with 10% heat inactivated fetal bovine serum (FBS) (Thermo Fisher Scientific, Gothenberg, Sweden), 10 U/mL Penicillin/Streptomycin (Thermo Fisher Scientific, Dartford, UK), and 1 X GlutaMax (Gibco, Thermo Fisher Scientific). Cells were grown at 6×10^6 density in 100 × 20 mm tissue culture treated petri dish (CytoOne®, Starlab, Hamburg, Germany) and maintained at 37°C in a humidified atmosphere with 5% CO_2. These cells were used as positive controls for glucocorticoid receptor expression, particularly NR3C1.

2.1.3 | Fibroblast culturing

A human primary fibroblast line was maintained in Dulbecco's Modified Eagle's Medium with 10% heat inactivated FBS (Thermo Fisher Scientific, Gothenberg, Sweden), 10 U/mL Penicillin/Streptomycin (Thermo Fisher Scientific, Dartford, UK). Cells were grown in a 75 cm^2 flask (Falcon®, Corning Life Science, Flintshire) and maintained at 37°C in a humidified atmosphere with 5% CO_2. The cells were used with iPSC as positive controls for a relative average telomere assay.

All cell lines were mycoplasma-tested before use according to the manufacturer's instructions (Mycoalert Detection Kit, Lonza).

2.2 | Assessment of cell death

Cells were stained for 15 min with Hoechst 33342 (5 μg/ml) to obtain the number of cells present on the coverslip, plus calcein-AM (calcein) to obtain the number of live cells (stained green with calcein-AM, 5 μM) and propidium iodide (PI, 5 μg/ml) to obtain the number of dead cells (staining red) which represent end-state apoptosis or necrotic cells, as previously described (Davenport et al., 2010). A minimum of 3 fields per coverslip were counted, and at least 3 coverslips were assessed for each variable per experiment.

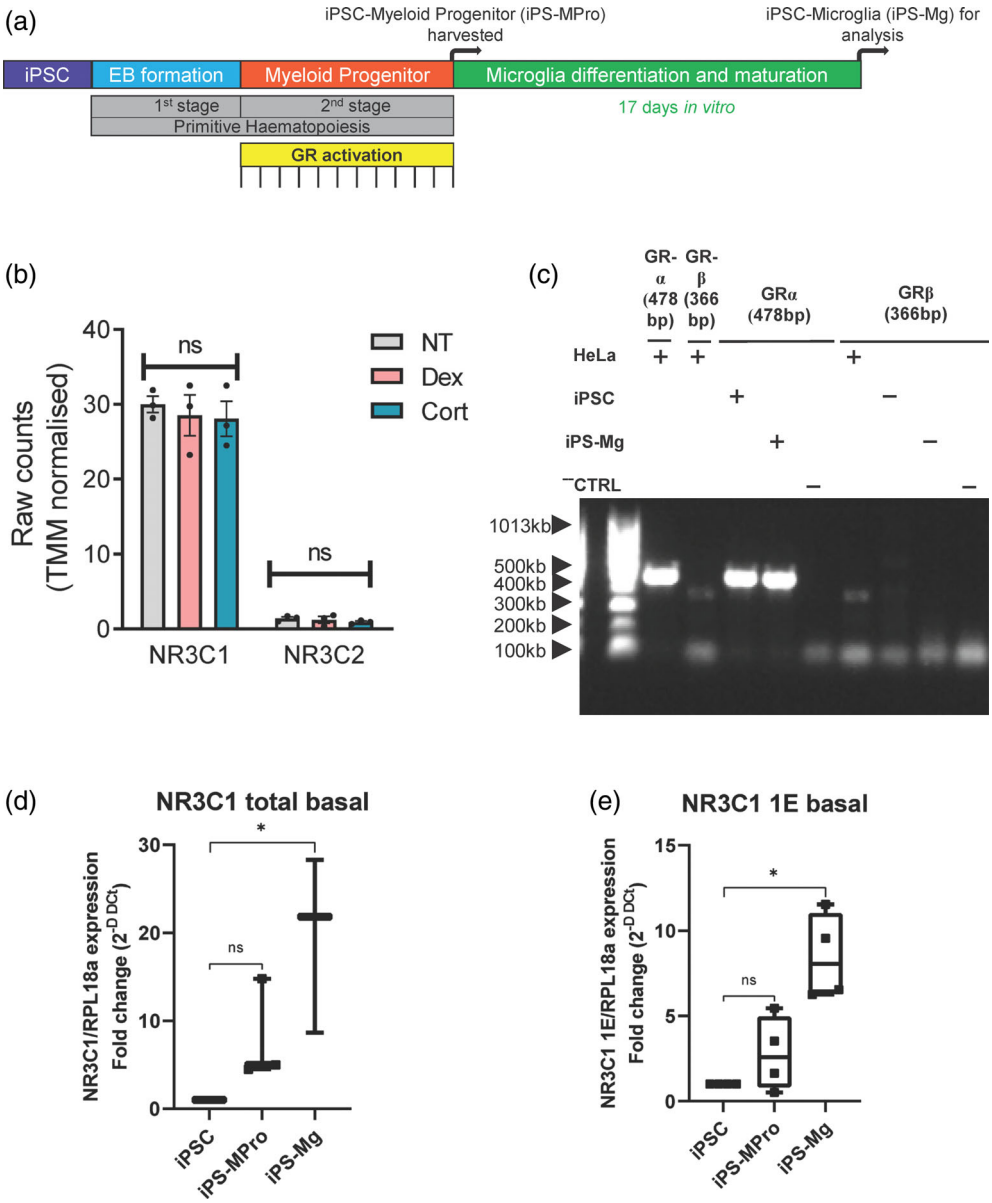

FIGURE 1 Treatment paradigm for iPSC-MPro and subsequent GR mRNA expression in iPS-Mg. (a) Treatment paradigm for ELS via GR stimulation; the GR agonist or anatagonist (i.e., Dex, Cort, RU486) was added into the medium every week for approximately 12 weeks as indicated, when the medium was replenished. The iPS-myeloid progenitors (iPS-MPro) were harvested and differentiated into microglia (iPSC-Mg). (b) Raw counts from RNA-seq analysis of GR NR3C1 and NR3C2 expressed in the iPS-Mg following no pretreatment of iPS-MPro control cells (NT), or pretreatment with dexamethasome (Dex) or hydrocortisone (Cort). $N = 3$. Kruskal-Wallis tests with Dunn's multiple comparison test. Data are the mean ± SEM. (c) iPSC and iPS-Mg expression of GR-α, and GR-β splice variant mRNA by PCR against the positive control HeLa. (d) Expression of NR3C1 mRNA in iPSC, iPSC-MPro and iPSC-Mg. $N = 3$. Kruskal-Wallis tests with Dunn's multiple comparison test where $^*p < .05$. Box-and-whisker plot representing all data points and the median. (e) Expression of NR3C1 1E mRNA in iPSC, iPSC-MPro and iPSC-Mg. $N = 4$. Kruskal-Wallis tests with Dunn's multiple comparison test where $^*p < .05$. Box-and-whisker plot representing all data points and the median

2.3 | Crude cytosolic/nuclear fractionation

Cytoplasmic fractionation was performed to analyze the presence of cytosolic DNA and was carried out according to Song et al. (2019), with minor modifications. Briefly, 1 million cells were harvested and lysed for 5 min on ice in 250 µl of cytoplasmic fraction buffer 10 mM HEPES, 10 mM KCl, 1.5 mM $MgCl_2$, 0.34 M sucrose, 10% (v/v) glycerol, pH 7.0–7.6 plus Halt™ protease and phosphatase inhibitor cocktail (Thermo Fisher Scientific, Dartford, UK). Subsequently, the pelleted nuclei were removed by low-speed centrifugation (1500 g, 10 min, 4°C). Then 200 µl of the cytoplasmic fraction was processed for genomic DNA extraction using the commercial PureLink™ genomic DNA Mini kit (Invitrogen, Thermo Fisher Scientific) according to the manufacturer's instructions. 10 µl of the cytoplasmic fraction was analyzed by BCA assay to normalize cytoplasmic DNA loading to cellular protein. Subsequently, an appropriate volume of the nuclear fraction

TABLE 1 Primer information for GR analysis

Primers	Forward sequence	Reverse sequence	Size/base pair
GRα	CCT AAG GAC GGT CTG AAG AGC	GCC AAG TCT TGG CCC TCT AT	478
GRβ	CCT AAG GAC GGT CTG AAG AGC	CCA CGT ATC CTA AAA GGG CAC	366
GR total	AGA GCA GTG GAA GGA CAG	GTT TTG TTA CCA GGA TTT TC	218
GR 1E	CAA CTT CCT TCG AGT TTG A	CAC AGT AGC TCC TCC TCT TA	299

TABLE 2 Taqman probs used for qPCR

Gene name	Assay ID
IFI6	Hs00242571_m1
IFI27	Hs01086373_g1
SAMD9L	Hs00970396_g1
FKBP5	Hs01561006_m1
TMEM119	Hs01938722_u1
GAPDH	Hs02758991_g1

to provide a positive DNA signal was suspended in 200 µl of PBS and genomic DNA extraction performed. Finally, DNA gel loading dye (Thermo Scientific™, Dartford, UK) was added into the cytoplasmic and nuclear extracts to stain the genomic DNA, and the cytoplasmic DNA concentrations were adjusted according to the protein concentration of cytoplasmic fractions and analyzed on a 1%–2% agarose gel.

2.4 | PCR and quantitative PCR

2.4.1 | PCR of GR expression

Cells were plated at 5×10^5 per well on a 6-well culture plate. RNA was extracted using RNeasy Plus Minikits (Qiagen, Manchester, UK) and reverse transcribed (RT) with a high-capacity cDNA Reverse Transcription kit (Applied Biosystems, Thermo Fisher). Commercially purchased human primary microglia cDNA (ScienCell, Carlsbad) was also analyzed as a control sample. For PCR analysis of GR-α and β, the PCR master mix (New England Biolab, Hitchin, UK) was prepared according to the manufacturer's instruction. One µl of cDNA from each sample was used for the amplification of the specific sequences of the GR spice variant. The primers used for GRα and GRβ were purchased from Integrated DNA Technologies (IDT, Belgium), GR total from SelectScience® (Merck), are listed in Table 1. Primer specificity and effieincy of GR total and 1 E were checked.

For analyzing GR total expression, qPCR was performed using qPCR Power SYBR™ Green PCR Master Mix (4367659, Applied Biosystems™) and GR total primer listed in Table 1, and a QuantStudio™ 7 Flex Real-Time PCR system (Applied Biosystems™).

qPCR was carried out using TaqMan Universal Mastermix (4440038, Life Technologies) and using specific primers (Table 2) in the Stratagene Mx3000p qPCR system and MxPro qPCR software. Expression was normalized to GAPDH (Hs02758991_g1, Applied Biosystems™).

2.4.2 | Relative telomere length measurement using qPCR

Using the crude cytosolic/nuclear fractionation, the nuclear fraction was further purified with 200 µl of PBS (with $MgCl_2$ and $CaCl_2$) for 5 min at 900 g to pellet the nuclear fraction further. This is to minimize confounding signals from the micronuclei present in the cytosolic fraction, as micronuclei contain a telomere signal (Norppa & Falck, 2003). The purified nuclear fraction was then used for the telomere assay.

Average telomere measurements using qPCR have previously been described (Cawthon, 2002; Joglekar et al., 2020). We followed the same protocol as Joglekar et al. (2020) and chose the single-copy gene (36B4) as a reference based on its primer specificity and efficiency (Table 3). After thermal cycling was completed, Agilent Aria 1.8 software was used to generate Ct values for telomere signals and reference gene signals. Average Ct value from three technical replicate was input for evaluation of relative telomere length as previously described (Vasilishina et al., 2019). Telomere to Single copy gene ratio (T/S ratio) was first calculated, then normalized to Ct value of reference DNA sample. Old-age human primary fibroblasts and iPSC were used as positive controls for the telomere length assay. Ct values of telomere and reference signals from iPSC served as a reference DNA sample.

2.5 | Immunocytochemistry of micronuclei

Cells were typically plated at a density of 2×10^4 on glass coverslips in 24 well plates. To stain for micro- nuclei, two antibodies were used, lamin a/c and cGAS. Cells was costained with antibody to P2Y12 to delineate the cytoplasmic space. iPS-Mg were fixed in ice-cold PBS with 4% paraformaldehyde (PFA) for 15 min. The cells were quenched in 50 mM NH_4Cl for 10 min, followed by permeabilisation with 0.2% Triton X-100 for 5 min. Primary antibody to lamin a/c (Abcam, Cambridge, UK) at 1:200 dilution was incubated overnight at 4°C in 5% normal goat serum followed by an appropriate secondary fluorescence- conjugated antibody. To stain for cGAS, cells were fixed in ice cold 100% methanol at −20°C for 5–7 min followed by 2 min

Primers	Sequence	Based on
36B4u	CAGCAAGTGGGAAGGTGTAATCC	Cawthon (2002)
36B4d	CCCATTCTATCATCAACGGGTACAA	
Tel A	CGGTTTGTTTGGGTTTGGGTTTGGGTTTG GGTTTGGGTT	Joglekar et al. (2020)
Tel B	GGCTTGCCTTACCCTTACCCTTACCCTTA CCCTTACCCT	

TABLE 3 Primers used for telomere qPCR assay

TABLE 4 Antibodies used for Western blotting

Target	Cat No	Supplier	Dilution
GAPDH	AM4300	Invitrogen	1:1000
Lamin a/c	Ab238303	Abcam	1:1000
Goat Anti-mouse 680	A21058	Invitrogen	1:1000
Goat Anti-mouse 790	A11357	Invitrogen	1:1000

brief permeabilization with 0.2% Triton X-100 in PBS. Primary antibody to cGAS (Santa Cruz Biotechnology, Texas) and P2RY12 (ATLAS, Stockholm, Sweden) at 1:200 dilution was incubated overnight at 4°C in 5% normal goat serum followed by an appropriate secondary fluorescence- conjugated antibody.

Secondary antibodies used were, goat anti-mouse-488 (Life Technologies, Thermo Fisher), or goat anti- rabbit-568 (Life Technologies, Thermo Fisher) at 1:500 dilution for 1 h at RT and nuclei and micronuclei were counterstained with DAPI (1 μg/ml of 4′,6-diamidino-2-phenylindole dihydrochloride in Vectashield Antifade Mounting Medium with DAPI). All images were acquired on a Zeiss LSM710 confocal microscope using the LSM Pascal 5.0 software. One hundred 63× magnification tiles from 5–8 random fields of each coverslip were captured. Images were analyzed in ZEN 3.4 (blue edition) software, and co- localisation of lamin a/c with micronuclei or co-localisation of cGAS with micronuclei were manually counted. More than 1500 cells from each condition were counted for lamin a/c and micronuclei; and over 4700 cells from each condition were counted for cGAS with micronuclei. Only non-apoptotic and non- necrotic cells were analyzed. Micronuclei classification was defined by criteria based on Ye et al. (2019).

2.6 | Immunoblotting

Immunoblotting was performed to determine the expression of lamin a/c and GAPDH. Typically, 20–40 μl of cytosolic and 60 μl nuclear fraction (isolated as above) were denatured and resolved by SDS-PAGE, transferred onto nitrocellulose membranes and incubated with primary and secondary antibodies (Table 4). To eliminate the possible interference with the protein, presence of DNA in the cytosolic fraction was eliminated using 10 μl of DNase I (Thermo Fisher Scientific, Dartford, UK). Proteins were visualized with an Odyssey detection system (LI-COR) and quantified using ImageJ software (www.imagej.nih.gov/ij).

2.7 | Analysis of senescence

2.7.1 | Senescence-associated β galactosidase staining

Senescence was determined with a Senescence Detection Kit (BioVision, Mountain View, CA), according to the manufacturer's instructions to detect senescence associated β-galactosidase activity (SA-β-gal). A minimum of 5–7 fields of view, in 2 biological replicates, repeated in 4 independent experiments were collected using Zeiss Axiophot light microscope (Carl Zeiss, Oberkochen, Germany) and photographed with a Nikon D300 camera (Nikon Instruments, Melville, NY), equipped with camera control pro 2 software. All images were converted to gray-scale and the same intensity threshold level was set for each image from each experiment. Mean β-gal activity in each field was calculated by using the mean gray value per field divided by the cell number counted per field.

2.7.2 | Senescence associated secretory phenotype

IPS-Mg medium supernatants from 2–3 independent experiments were collected, centrifuged at 300 g for 10 min at 4°C, to remove debris and processed according to the manufacturers' instructions (Proteome Profiler™ Human XL cytokine array kit; R&D Systems, Abingdon, UK). In total, supernatants pooled from 2–3 biological replicates from NT, Dex, or RU/Dex pre-treated microglia were incubated per membrane, for a total of 2 membranes per condition. Each membrane was imaged with an Odyssey FC (Li-Cor Biosciences), and dot density quantified in Image studio Lite Version 5.2, normalizing to both reference and negative control dots.

2.7.3 | Ki-67 proliferation assay

1×10^6 iPS-MPro were collected from the flasks and plated on 100 × 20 mm tissue culture treated petri dishes for 72 h to proliferate over a large surface area. Cells were fixed using 80% ethanol and left at −20°C for 1 h before staining. Cells were stained with FITC-conjugated anti-Ki-67 antibody (Miltenyi Biotec, Germany) as per manufacturer's protocol. To rule out unspecific binding of the Ki-67 antibody, an isotype control antibody was used (1:50 dilution, REA control antibody, Miltenyi Biotec, Germany). Samples were analyzed

using a flow cytometer (Becton Dickinson FACSCalibur). At least 10,000 events were acquired per condition and data analyzed with Flowing software 2.5.1, (University of Turku, Finland).

2.8 | RNA-seq

2.8.1 | Bulk cells RNA-seq

Total cellular RNA was extracted using the RNeasy Plus Mini Kit (Qiagen, Manchester, UK) according to the manufacturer's instruction with minor modifications. Multiple replicates from each cell line and each condition were pooled together for RNA extraction and RNA from all samples was submitted to UCL Genomics processing (Zayed Center for Research into Rare Disease in Children, 20 Guilford Street, London WC1N 1DZ). The concentration and quality (integrity) of the total RNA was determined using a TapeStation System (Agilent) and the RIN (RNA Integrity Number) Quality Metric. RIN values of all samples sent for RNA-Seq were above 7. Thus, 500 ng of RNA were enriched for polyA tailed mRNA, fragmented, reverse transcribed and ligated to index sequencing adapters using Kapa mRNA HyperPrep kit (Roche) according to the manufacturer's instructions. Amplified libraries were then sequenced on a NovaSeq 6000 SP flow-cell generating 20–25 million reads with 100 bp single-end reads.

2.8.2 | Analysis of RNA-seq

Raw RNA-seq reads were processed for quality check and adapter trimming using fastp, then aligned to the ensemble human reference GRCh38 genome using HISAT2 (version 2.2.1) (Kim et al., 2019). Gene expression was subsequently quantified using the featureCounts function within Rsubread (version 1.34.7) (Liao et al., 2014; Liao et al., 2019). Then, the raw gene counts were processed with the DESeq2 package (version 1.26.0) (Love et al., 2014) in R (version 3.6.1) to analyze differentially expressed genes (DEGs). Gene Ontology enrichment analysis of DEGs was performed in R using the package clusterProfiler (version 3.14.3, qvalueCutoff = 0.05) (Yu et al., 2012). GSEA analysis of the transcriptome was also performed in R using the package clusterProfiler.

2.8.3 | Transcriptomic comparative analysis of in-house iPS-Mg and human primary microglia

Raw FASTQ files of ex vivo human primary microglia from different ages (0.42–90 years old) (Galatro et al., 2017; Gosselin et al., 2017; Olah et al., 2018; Zhang et al., 2016) were downloaded and input for downstream analysis using the same pipeline as our in-house iPS-Mg RNA-seq data. Briefly, FASTQ files were processed for quality check and adapter trimming using fastp, then pseudo-mapped to the human transcriptome (human Gencode release 36) using Salmon (version 1.4.0). Tximport was then used to import Salmon's transcript-level quantifications and aggregate them to the gene level quantification. The size and depth of the sequencing library per sample and the length of the genes were then normalized using the normalization Factors function within DESeq2. Similarity and distance among samples from different ages of primary microglia and in-house iPS-Mg were assessed using the R default dist function. Before performing sample distances, counts underwent variance stabilizing transformation.

2.8.4 | Comparative pathway enrichment analysis of in vitro and in vivo model of ELS

To identify pathway enrichments, differentially expressed genes from in house iPSC-Mg treated with Cort were submitted for PANTHER over-representation analysis. A comparable analysis was performed on in vivo ELS data (Delpech et al., 2016).

2.8.5 | Weighted gene co-expression network analysis

The featureCount processed genes matrix from the RNA-Seq analysis was first filtered for missing values and zero-variance-genes using the goodSamplesGenes function, and then 36,599 genes were included in the WGCNA analysis. One signed network was constructed using the WGCNA package in the R language (Langfelder & Horvath, 2008), with GR activation and genotype as traits. Thus, we performed the analysis of network topology for various soft-thresholding powers to have relative balanced scale independence and mean connectivity of the WGCNA. Finally, the network construction and module detection followed these default parameters: Pearson's correlations, power of 12, maxBlockSize of 100,000, minModuleSize of 10, deepSplit of 2, and mergeCutHeight of 0.25.

To ensure that the modules identified were indeed associated with the traits, we first determine module significance (MS), which can be defined as the average gene significance (GS) across module genes. GS is a term that refers to the relationship between an individual gene and a biological trait. Thus, modules with a higher mean GS indicate a greater degree of association between the module's genes and the traits. For the purpose of selecting gene modules of interest, we compared the average GS of the modules. Second, we created a scatter plot of the module membership (MM) versus the GS. Module membership (MM) is defined by WGCNA as MM (i) = cor (x_i, ME), and it is used to quantify a gene's importance within a module.

This is to show that within each module, the genes that are associated with the trait are also the inevitable components of the modules. For instance, if GS and MM were highly correlated, this indicated that genes were critical components of modules and were highly correlated with the trait (Langfelder & Horvath, 2008). The Zsummary. qual module quality and robustness metric was developed by performing a module preservation analysis on a single network as a test and reference (Langfelder et al., 2011). The modules were functionally

annotated using the Gene Ontology enrichment analysis function in R, which is included in the package clusterProfiler (version 3.14.3, qvalueCutoff = 0.05).

2.9 | Statistical analysis

Statistical analysis was carried out in GraphPad Prism using unpaired t-test, Mann–Whitney *U* test, ANOVAs (one-way) and Krushal-Wallis test with Dunn's multiple comparison tests from at least 3 independent experiments. Statistical significance was defined as $^{*}p < .05$, $^{**}p < .01$, $^{***}p < .005$. The application of the statistical analysis test was pre-determined by normality testing conducted in Prism.

3 | RESULTS

3.1 | iPSC and iPS-Mg expressed glucocorticoid receptor, but not mineralocorticoid receptor at mRNA level

The physiological receptors for GCs are glucocorticoid receptor (GR) and mineralocorticoid receptor (MR) (Timmermans et al., 2019). We determined by RNA-seq that human iPS-Mg predominately expressed glucocorticoid receptor (NR3C1), and less mineralocorticoid receptor (NR3C2) (Figure 1b,c). The NR3C1 expression level was independent of cell treatment and NR3C2 expression was not altered by treatment (Figure 1b). We then determined that the predominant splice variant of the GR was GR-α, and this was present in both iPSC and iPS-Mg, while GR-β was not present in either the iPSC or the iPS-Mg (Figure 1c). Because Lieberman et al. (2017) demonstrated that GR mRNA expression levels increased during neural differentiation, we asked whether a similar trend was observed during the differentiation of our iPS-Mg. Since GR exon 2–8 does not undergo splice variant events, and most of the GR protein isoforms originate from one species of mRNA GR (Lu & Cidlowski, 2005), we used exon 7 as a readout of GR mRNA total expression. We found that there was a significant differentiation related increment in NR3C1 mRNA expression from iPSC to iPS-Mg (Figure 1d) Interestingly the splice variant 1E within the 5′ untranslated region (UTR) of the GR was not expressed in the iPSC but was significantly expressed (as shown by qPCR) in the matured iPS-microglia (Figure 1e). The GR 1E within the 5' UTR of GR is expressed predominantly in immune cells, indicating a differential maturation of our cells from iPSC to microglia (Turner & Muller, 2005).

3.2 | The transcriptomic profile of iPS-Mg cluster closely with primary human young microglia

To determine the validity of using our iPS-Mg to model GR related ELS, we asked whether the microglia resembled microglia from a young age. We integrated publicly available transcriptomic data on human primary microglia from different ages across a life span of 0.42–90 years of age (Galatro et al., 2017; Gosselin et al., 2017; Olah et al., 2018; Zhang et al., 2016) and compared this with our iPS-Mg using a hierarchical clustering method (Euclidean distance). We found that the transcriptomic profile of our human iPS-Mg clustered with young microglia (Figure 2a). This is in line with other papers (Abud et al., 2017; Haenseler et al., 2017). These findings thus verified the use of our human iPS-Mg to model the impact of ELS at a relevant biological age.

3.3 | The comparative analysis of iPS-Mg ELS model and in vivo ELS model

A characteristic of a murine in vivo ELS model (prenatal viral infection) was the significant upregulation of TMEM119 (Ozaki et al., 2020). Assessment of TMEM119 mRNA in our ELS exposed iPS-Mg mirrored this (Figure 2b) and was the only microglial signature gene which was upregulated (Figure 2c). Taken together, these data suggest that our in vitro model of ELS may mimic certain biological consequences associated with experimental ELS in vivo.

To assess whether our model of ELS can recapitulate the biological consequences of ELS in vivo, we conducted pathway enrichment analysis of the transcriptomic data from our ELS model and a rodent model of ELS (Delpech et al., 2016). Interestingly, the interferon alpha/beta signaling pathway and its associated pathways were found to overlap in both our ELS and an in vivo model of ELS (Delpech et al., 2016) (Table 5). Additionally, significant upregulation of FKBP5 mRNA, a co-chaperone of GRs (Binder, 2009), has been observed in adult mice exposed to an adverse early life environment at an embryonic stage (Ke et al., 2018). Here the same pattern of upregulated FKBP5 mRNA was also found in our model Dex-iPS-Mg (Figure 2d) and Cort-iPS-Mg (Supplementary Figure 1e). Specifically, not only the total FKBP5 mRNA was upregulated (Figure 2di), but also its splice variant FKBP5-201 (Figure 2dii) and FKBP5-204 (Figure 2diii). The expression profile of FKBP5 gene in NT- and Dex-iPS-Mg was independently verified by TaqMan qPCR assay (Supplementary Figure 1d).

Sequence homology analysis was performed by using BLAST to align human FKBP5-201 transcript sequence (GRCh38) to mouse genome (GRCm39). The result yields an identity score of 85.05% between human FKBP-201 transcript (ENST00000357266.9), and mouse FKBP-201 transcript (ENSMUST00000079413.11) as the top one significant alignment hit. This suggests that human and mouse FKBP5-201 have an identify score of 85.05% and is highly conserved which facilitated the direct comparison between the expression level of FKBP5-201 in both human and mouse (Table 6). The RNA- Seq of NT-iPS-Mg and Dex-iPS-Mg raw reads mapped onto FKBP-201 transcript are shown in a Sashimi plot (Figure 2e).

3.4 | Chronic GR activation during primitive hematopoiesis triggers enhanced expression of type I interferon-stimulated genes

We found five of the commonly defined type I interferon (IFN)-induced genes (database from Gene Ontology) were significantly differentially expressed (DE) in the Dex pre-exposed iPS-Mg compared with NT iPS-

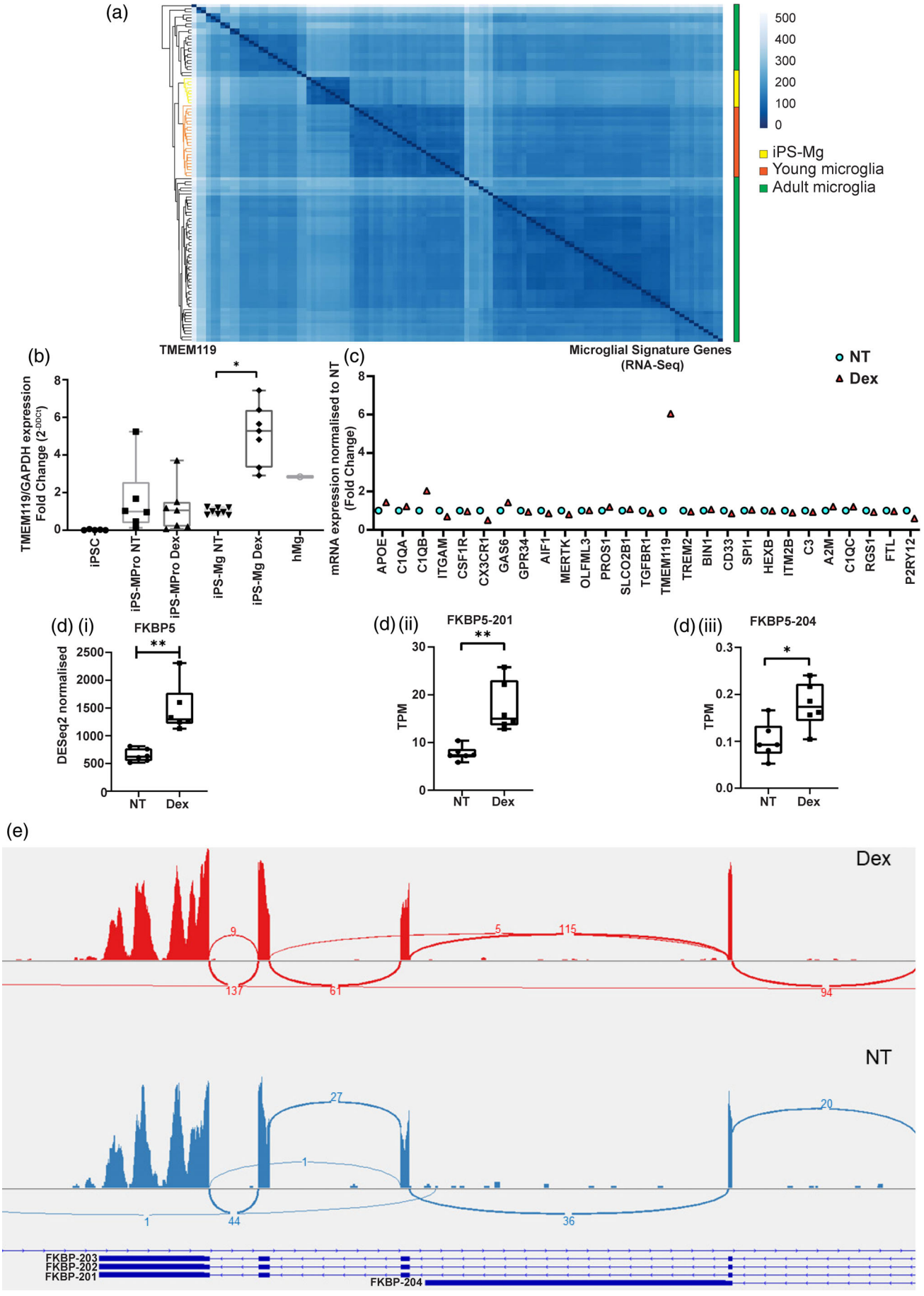

FIGURE 2 Legend on next page.

TABLE 5 Pathway enrichment analysis between our ELS model and Delpech et al., 2016; ELS microarray gene expression data

Network cluster enrichment	FDR
Interferon alpha/beta signaling	6.11E-14
Interferon alpha/beta signaling, and Interferon gamma signaling	1.4E-13
Type I interferon signaling pathway	1.13E-12
2′-5′-oligoadenylate synthase, and type I interferon signaling pathway	2.97E-12
Mixed, incl. 4Fe-4 S single cluster domain, and IFN-induced protein with tetratricopeptide repeats 3	0.000000193
Collagen biosynthesis and modifying enzymes, and Elastic fiber formation	0.0056
Delpech et al. 2016: Network Cluster Enrichment	
Toll-like receptor signaling pathway, and Activation of IRF3/IRF7 mediated by TBK1/IKK epsilon	9.21E-17
TIR domain, and interleukin-1-mediated signaling pathway	9.34E-10
Activation of IRF3/IRF7 mediated by TBK1/IKK epsilon	2.40E-07
TNFSF members mediating non-canonical NF-kB pathway, and TNFα	3.44E-07
SMAD protein complex assembly, and c-SKI Smad4 binding domain	5.04E-06
Regulation of IFNG signaling, and interleukin-6 receptor complex	7.12E-06
Type I interferon signaling pathway, and type I interferon receptor binding	0.00012
Growth hormone receptor signaling pathway via JAK-STAT, and Leptin	0.0128
Type I interferon biosynthetic process, and Interferon beta	0.0128

TABLE 6 Sequence homology analysis using BLAST

Transcript ID	Transcript ID	Identities
ENST00000357266.9	ENSMUS 00000079413.11	(85.05%)

Mg, such as the following interferon-stimulated genes (ISG) IFI6, IFI27, MX1, IFIT3, SAMD9L (adjusted ρ < .1, |log2 fold-change| > 1), (Figure 3a). The expression profile of three top ISG genes in NT- and Dex-iPS-Mg was independently verified by TaqMan qPCR assay (Supplementary Figure 1a–c). Interestingly, SAMD9L and IFI27 transcripts were significantly enriched in micronuclei containing cells (Mackenzie et al., 2017). This led us to ask if certain ISG-related signaling pathways were activated after Dex exposure and thus assessed the Dex specific upregulation of commonly defined type I IFN-induced genes on a transcriptome-wide basis. Gene set enrichment analysis (GSEA) against all genes ranked by z-scores for differential expression (Dex versus NT) calculated by DESeq2 package in R. GSEA confirmed that not only type I interferon genes are enriched in Dex-iPS-Mg (FDR = 0.0065) (Figure 3b) but also innate immune response genes are enriched (FDR = 0.0048) (Supplementary Figure 2).

To confirm these findings, an endogenous agonist of GR, hydrocortisone (Cort) was used in the same way as Dex treatment. Analysis of Cort-iPS-Mg revealed 125 significantly upregulated and 129 downregulated genes compared with NT iPS-Mg (adjusted p < .1, |log2 fold-change| > 1), (Figure 3c). Consistent with Dex-iPS-Mg, Gene Ontology analysis on the significantly DE genes affirmed activation of type I interferon signaling in Cort-iPS-Mg (Figure 3d).

To further validate the activation of type I interferon signaling when iPS-Mg were pre-exposed to GR, we tested our hypothesis on a different genetic background. Patient-derived iPS-Mg expressing the Alzheimer's Disease (AD) risk variant R47H^{het} in triggering receptor expressed on myeloid cells 2 (TREM2 R47H^{het}) were treated with Dex in the same manner as our control lines used above (SFC840, BIONi010-C, and KOLF2_C1) (Cosker et al., 2021; Piers et al., 2020). To gain an understanding of obvious and subtle changes, we performed weighted gene co-expression network analysis (WGCNA).

We integrated RNA-Seq of control lines and TREM2 variant lines +/− Dex, Cort into the WGCNA analysis (15 samples in total) and detected a total of 32 modules (Supplementary Figure 3).

For module-trait analysis, we categorized Dex and Cort and NT as the GR activation trait. First, this is because our previous analysis indicated that Dex and Cort treatment led to activation of similar pathways (Figure 3); second, in vitro studies of the pharmacological characteristics of Dex and Cort in cells expressing endogenous GR show that the concentrations of Cort or Dex used in the present study are at the receptor EC_{50} (Longui et al., 2005), which facilitates the combination of Cort and Dex, a GR activation trait for WGCNA.

Out of 32 detected modules, the module eigengene of 7 modules, namely royalblue, darkturquoise, green, red, darkgrey, yellow and purple were significantly correlated with the GR activation trait (Figure 4a,

FIGURE 2 Comparative transcriptome analysis of iPS-Mg with publicly - available datasets for young and adult microglia. (a) Heatmap of transcriptomic profile of Euclidean distance between in-house iPS-Mg and ex vivo primary human microglia from different ages (Galatro et al., 2017; Gosselin et al., 2017; Olah et al., 2018; Zhang et al., 2016). (b) TMEM119 mRNA expression at different cell stages from iPSC to iPSC-Mg following ELS paradigm treatment. Box-and-whisker plot representing all data points and the median, where *p < .05. (c) RNA-seq of microglial signature genes showing increase in TMEM119 following Dex treatment. Data points are DESeq2 normalized fold change to NT from three biological replicates each condtion. (d) Expression of FKBP5 based on RNA-seq data analyses between NT and Dex pre-treated iPS-Mg. (i) Total FKBP5 in NT or Dex pre-treated iPS-Mg. Values are DESeq2 normalized data from RNA-seq data. (ii) Expression of FKBP5-201 splice variant in NT and Dex pre-treated iPS-Mg from RNA-seq data. (iii) Expression of FKBP5-204 splice variant in NT and and Dex pre-treated iPS-Mg from RNA-seq data. Values are from RNA-seq data and expressed as Salmon normalized TPM (transcript per million) counts. $N = 6$. Box-and-whisker plot representing all data points and the median. Unpaired t-tests and *p < .05, **p < .01. (e) IGV-Sashimi plot depicting the splice variants of FKBP5 and the number of reads mapped on exons of FKBP5 between NT (blue) and Dex iPS-Mg (red).

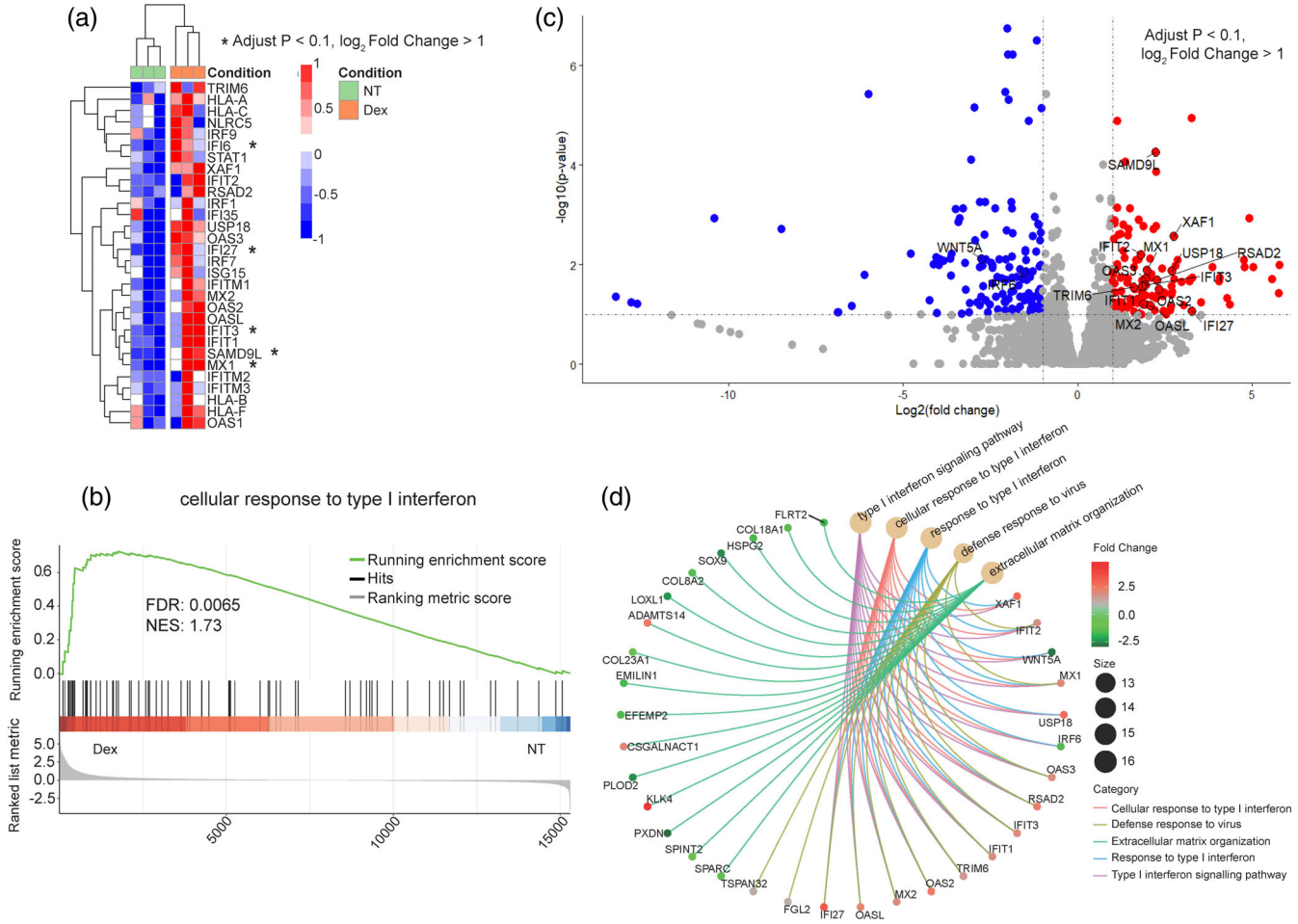

FIGURE 3 Transcriptomic analysis of Dex and Cort pre-exposed iPS-Mg. (a) Heatmap of type I IFN-induced genes in NT and Dex pre-exposed iPS-Mg. DESeq2 normalized data are plotted. * adjusted $p < .1$, |log2 fold-change| > 1. (b) Transcriptome-wide analysis (GSEA) of commonly defined type I IFN-induced genes (FDR = 0.0065) is significantly enriched in transcriptomes of Dex pre-exposed iPS-Mg. (c) Volcano plot illustrating differential expression of genes in Cort pre-exposed iPS-Mg and NT iPS-Mg. Genes with adjusted $p < .1$, and |log2 fold-change| > 1 are plotted in red and blue. Red indicates upregulation, blue indicates downregulation. Type I IFN-induced genes were circled. (d) Gene ontology analysis of the significantly differentially expressed genes, and significantly enriched signaling pathways in Cort pre-exposed iPS-Mg compared with NT iPS-Mg.

marked with*). Also, these 7 GR modules are not affected by the genetic variation between the control lines used here (which express the common TREM2 variant) and the R47H^{het} TREM2 variant lines.

By using gene significance (GS) and module membership (MM) analysis, we ensured that the GR modules are specific to GR activation traits (Supplementary 4a and Supplementary Figure 4b–h). To ensure the GR modules are high quality modules, we implemented module preservation analysis on one single topological overlap matrix (TOM) network both as test and reference. Since only one TOM was constructed, module quality was assessed in the present study. We calculated multiple module quality statistics that measure how well-defined modules are in repeated random splits of the reference dataset. All modules demonstrated strong evidence for high quality (Zsummary > 10), confirming that GR modules were well-defined and non-random (See Supplementary Figure 5a).

To gain a deep understanding of what GR pre-treatment does to iPS-Mg, we further analyzed the GR activation-related modules. Since genes that are highly co-expressed often share similar functions, biological processes and pathways that are enriched in a co-expression module can be used to infer functional information (de la Fuente, 2010; Singer et al., 2005). We performed Gene Ontology enrichment analysis on the 7 identified GR modules to detect significantly overrepresented gene ontology categories in each WGCNA module. The top three significant pathways in each module were plotted (Figure 4b). The purple module is enriched in pathways associated with defense responses to viruses (q.value = 7.59E-06), which confirmed the type I interferon signaling pathway identified in our DE gene analysis. The darkgray (q.value = 0.00553918), red (q.value = 2.45E-06) and yellow modules (q.value = 0.006206759) are significantly enriched with genes associated with macro-autophagy and the autophagy pathway. The green module is enriched with pathways associated with ribosome biogenesis (q.value = 2.00E-25), nuclear export (q.value = 4.41E-19) and non-coding RNA processing (5.62E-22 q.value).

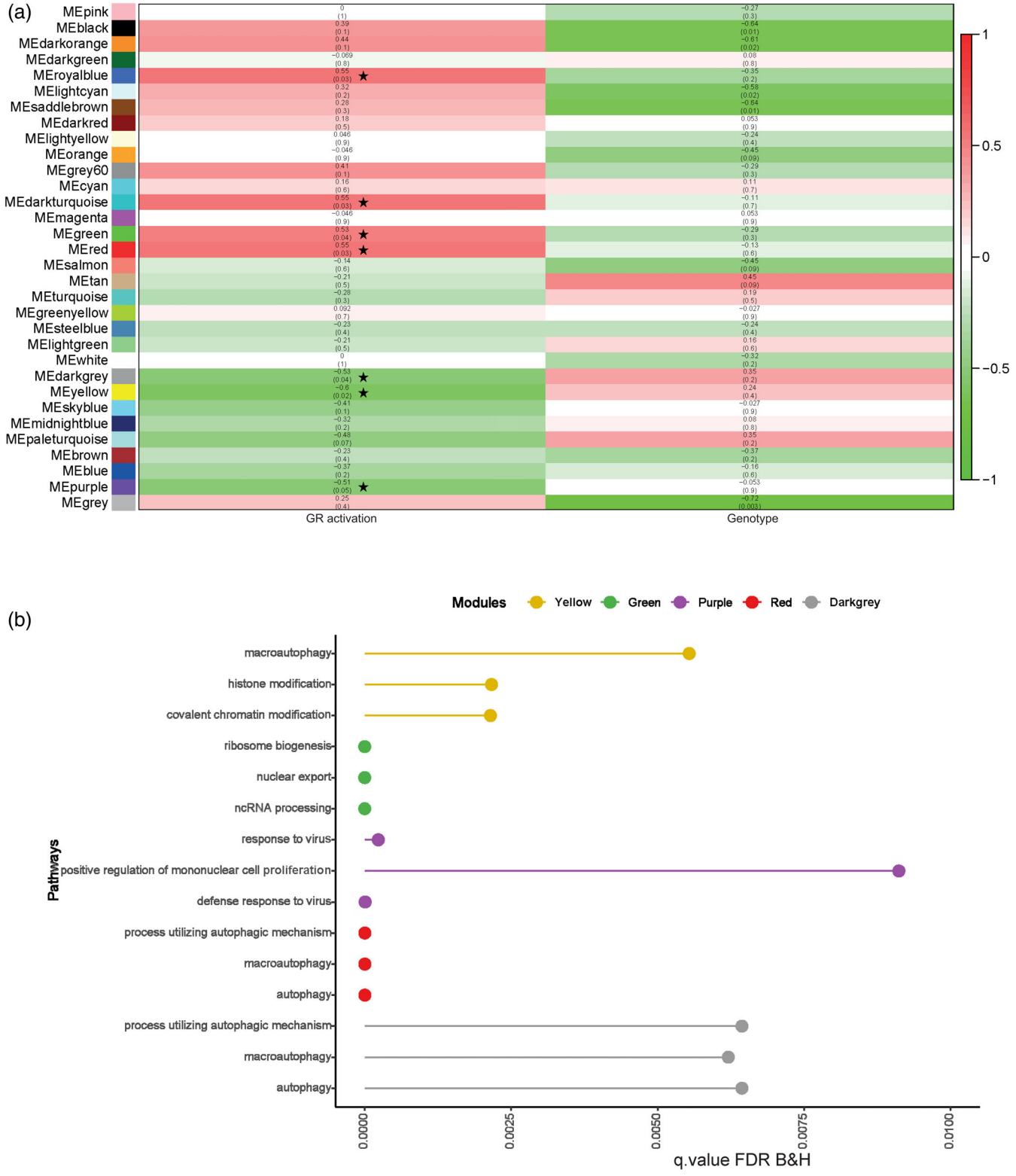

FIGURE 4 WGCNA analysis of Dex and Cort pre-exposed iPS-Mg with Cv and TREM2 variants. (a) Diagram of module-trait relationship reports Kendall's correlation coefficients (shown at the top of each row), and its corresponding p values (displayed at the bottom of each row within parentheses) between the eigengene value of each module, two traits GR activation and genotype are displayed at the bottom of the diagram as column. Modules specifically related to GR activation and were not correlated with genotype are marked with star. The direction of the correlation was color-coordinated with positive correlations indicated in red and negative correlation in blue. (b) GO enrichment analyses of genes in yellow, green, purple, red and darkgray modules, top 3 significantly enriched pathways in each pathway were plotted. Bars representing GO terms show Benjamini and Hochberg FDR adjusted p values (q.value).

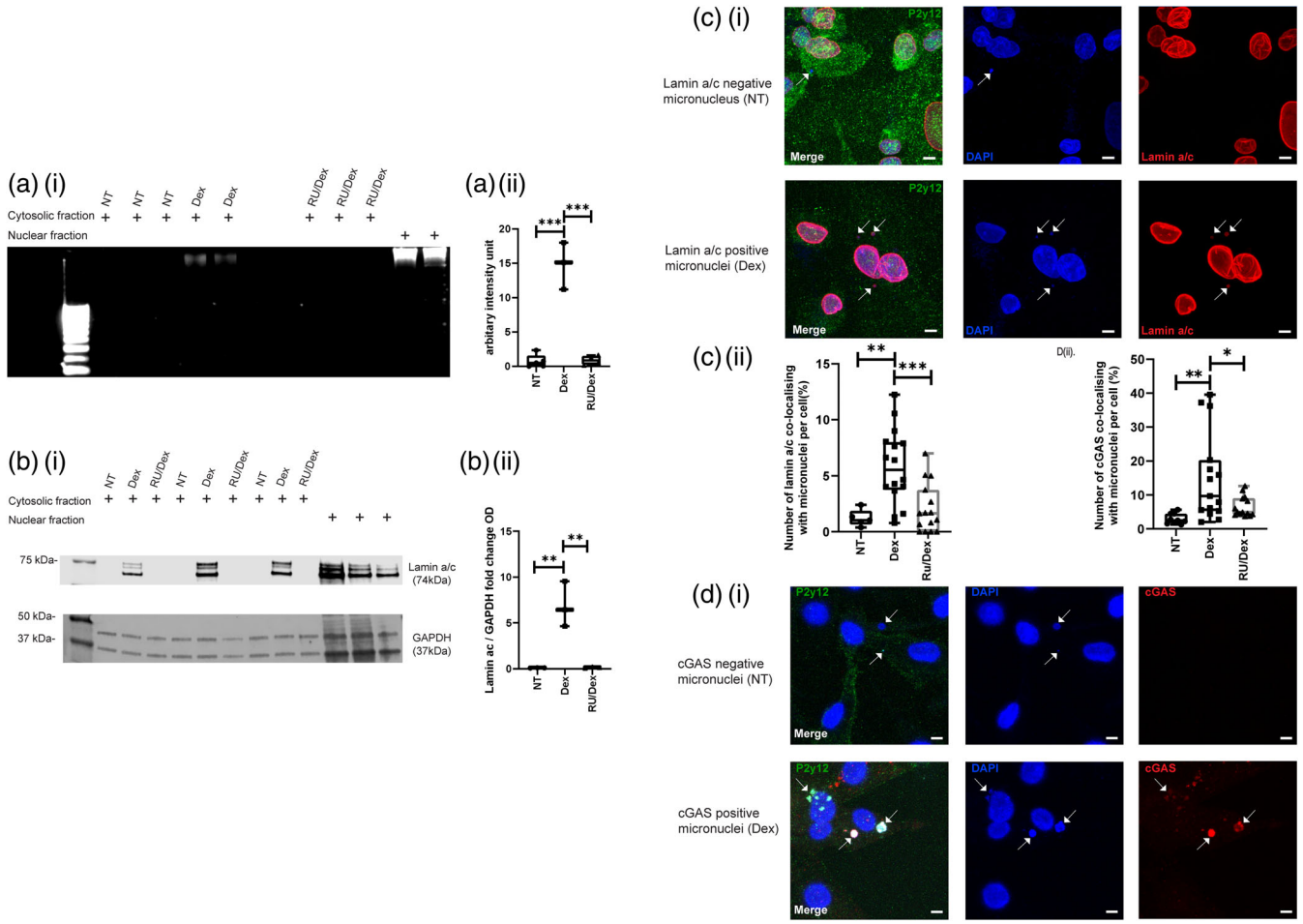

FIGURE 5 Formation of micronuclei and cGAS activation in Dex pre-exposed iPS-Mg. (ai) Agarose gel analysis of genomic DNA in cytosolic or nuclear extracts from NT iPS-Mg, Dex pre- treated iPS-Mg and RU/Dex pre-treated iPS-Mg. (aii). Quantification of the genomic DNA present in the cytosolic and nuclear fraction from the gel shown in ai. $N = 3$ biological replicates (additional replicates are shown in Supplementary Figure 5b. One-way ANOVA with Dunn's multiple comparison test. Box-and-whisker plot representing all data points and the median. (bi) Western blot of Lamin a/c in cytosolic and nuclear fractions. Nuclear fractions are shown as positive controls for Lamin a/c. GAPDH served as a loading control in the cytosolic extract. (bii) Quantification of Western blot shown in bi. $N = 3$ One-way ANOVA with Dunn's multiple comparison test. Box-and-whisker plot representing all data points and the median. (ci) Immunostaining with antibody against Lamin a/c (red), P2y12 (green) with DAPI nuclear counterstain (blue) in NT iPS-Mg, Dex pre-treated iPS-Mg; a representative image of RU/Dex pre-treated iPS-Mg is provided in Supplementary Figure 7. Scale bar: 5 µm. (cii) Number of micronuclei/cell in NT iPS-Mg (4 biological replicates), Dex pre-treated iPS-Mg (6 biological replicates, and RU/Dex pre-treated iPS-Mg (6 biological replicates). One-way ANOVA with Dunn's multiple comparison test. Box-and-whisker plot representing all data points and the median. Each data point represents one whole field of 10 × 10 tile scan per condition (100 individual pictures). Arrow points to lamin a/c positive and negative micronuclei. (di) Immunostaining with antibody against cGAS (red), P2y12 (green) with DAPI nuclear counterstain (blue) in NT iPS-Mg, Dex pre-treated iPS-Mg; a representative image of RU/Dex pre-treated iPS-Mg is provided in Supplementary Figure 8. Scale bar: 5 µm. (dii) Number of cGAS colocalising with micronuclei per cell in NT iPS-Mg, Dex pre-treated iPS-Mg and RU/Dex pre-treated iPS-Mg. $N = 3$ biological replicates, one-way ANOVA with Dunn's multiple comparison test to compare nontreated group with the Dex and RU/Dex pre-treated group, $^{*}p < .05$; $^{**}p < .01$; $^{***}p < .005$. Box-and-whisker plot representing all data points and the median. Each data point represents one whole field of 10 × 10 tile scan per condition (100 individual pictures). Arrow points to cGAS positive and negative micronuclei

Darkturquoise and royalblue yielded no significant pathways within the modules.

3.5 | Genomic self-DNA was found in Dex-iPS-Mg

To follow up on the finding of enhanced type I interferon and associated viral and viral defense signaling in Dex-iPS-Mg, we reasoned that one possible cause of this signal might be genomic self-DNA in the cytoplasm (Keating et al., 2011). In this ectopic location, the self-DNA would be perceived as an invading virus and trigger an anti-viral defense and transcription of type I interferon (Honda et al., 2006). We investigated the possible presence of cytosolic self-DNA. Following crude cytosolic/nuclear fractionation, we found that Dex-iPS-Mg displayed significantly more cytosolic self-DNA compared with NT-iPS-Mg or RU/De-iPS-Mg (Figure 5a,

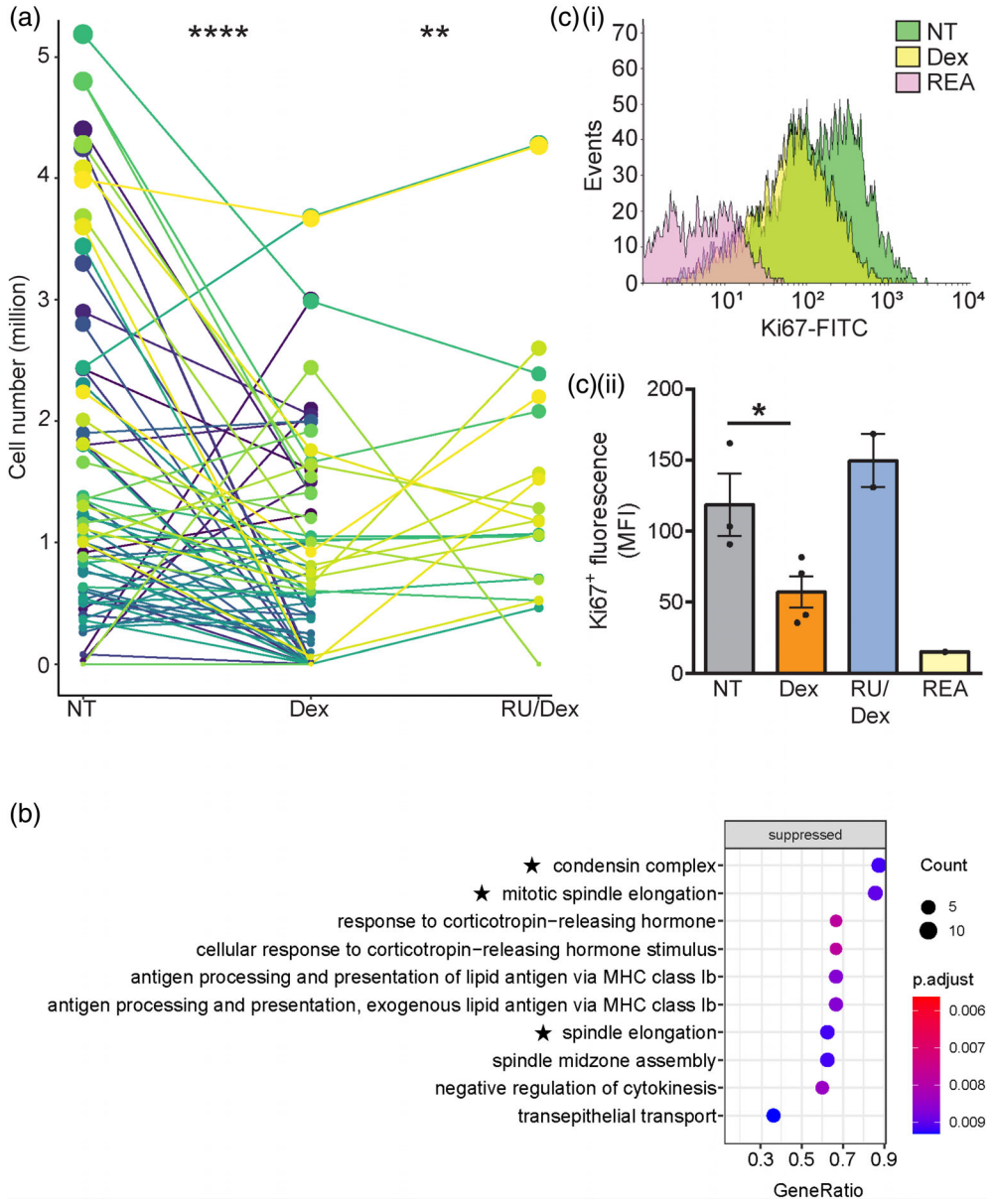

FIGURE 6 Dex-treated iPS-MPro and pre-treated iPS-Mg exhibit reduced cell number and proliferation. (a) Before-after graph of the iPS-MPro cell number generated during primitive hematopoiesis either non- treated (NT) or treated with Dex or Ru/Dex. Lines connected with dots across treatments mean one collection event. Kruskal-Wallis test with Dunn's multiple comparison test of NT versus Dex (****$p < .0001$) or Dex versus RU/Dex (**$p < .01$). (b) Dot plots of GSEA results illustrating top 10 GO biological processes and cellular components associated with consequences of Dex-pretreated iPS-Mg based on gene ratio. "Gene ratio" is the percentage of total DEGs in the given GO term (only input genes with at least one GO term annotation were included in the calculation). (ci) Representative FACS histogram of cells stained with anti-Ki67 antibody in NT, Dex and RU/Dex pre- treated iPS-Mg. (cii) Quantification of Ki-67 protein expression as mean fluorescent intensity (MFI) shown in c. Data are the mean of $n =$ at least 3, analyzed with Two-tailed unpaired t test. *$p < .05$. Data are the mean with ±SEM

Supplementary Figure 5b) and that this was prevented by RU treatment (Figure 5aii).

To ensure that the cytosolic extract was not contaminated by spill-over from the nuclear fraction, the cytosolic extract was probed for lamin a/c, a nuclear protein (Dubik & Mai, 2020). We found in NT-iPS- Mg, there was no lamin a/c, which confirmed that the cytosolic extract was not contaminated by the nuclear fraction. Conversely, there was significantly more lamin a/c in Dex-iPS-Mg, which was attenuated by pretreatment with GR antagonist RU486 (Figure 5bi,ii).

3.6 | Higher number of lamin a/c positive micronuclei and cGAS positive micronuclei were found in Dex-iPS-Mg

This finding led us to speculate that the cytosolic self-DNA with lamin a/c could be micronuclei (Kneissig et al., 2019). Micronuclei are lamin a/c positive small DNA-containing nuclear structures that are spatially isolated from the main nucleus (Kwon et al., 2020). Confocal imaging analysis revealed that Dex-iPS-Mg displayed significantly more micronuclei per cell compared with NT-iPS-Mg or RU/Dex-iPS-Mg (Figure 5c). To ensure that we do not mistake apoptotic bodies as micronuclei, we ensured that pre-treated of Dex or RU486 alone do not induce significant cell death (Supplementary Figure 6a,b).

Micronuclei are susceptible to nuclear envelope collapse (Hatch et al., 2013) due to an unstable micronuclei envelope. The DNA in the micronuclei can serve as a source of immunostimulatory cytosolic DNA. Following this, cyclic GMP-AMP synthase (cGAS) binds to self-exposed DNA in the micronuclei, 2′-5'-cGAMP is synthesized, leading to the activation of stimulator of interferon genes (STING) and transcription of type I interferon (Zierhut & Funabiki, 2020). Since cGAS is upstream of this pathway, and cGAS localizes to micronuclei upon nuclear envelope rupture (Mackenzie et al., 2017), we investigated the number of cGAS colocalised micronuclei per cell in NT-, Dex- and

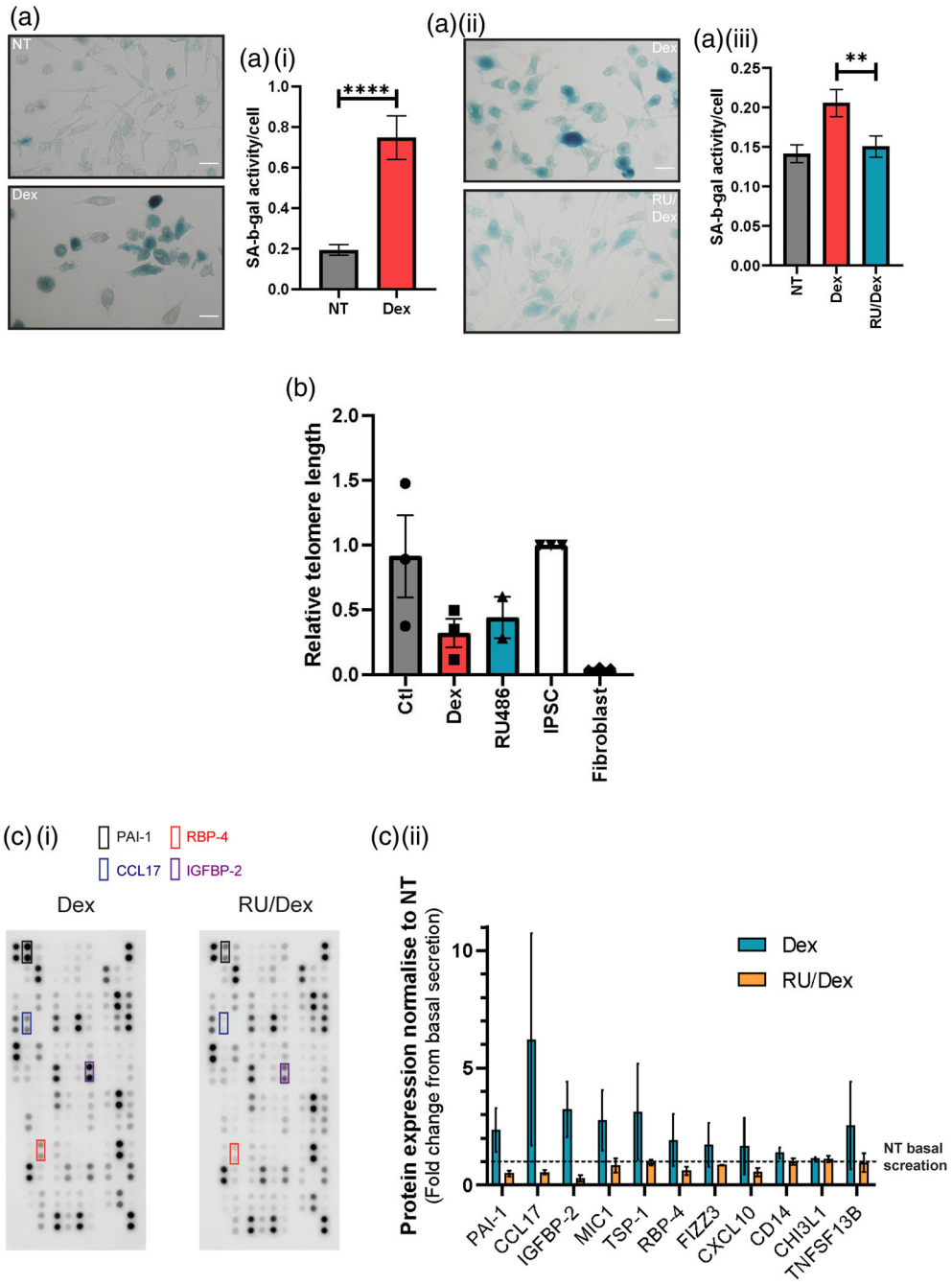

FIGURE 7 Dex-pre-treated iPS-Mg exhibit characteristics of cellular senescence. (a) Representative images of senescence-associated beta galactosidase (SA-β-gal) staining in NT and Dex pre-treated iPS-Mg. (ai) SA-β-gal activity quantified by staining intensity in NT, Dex pre-treated iPS-Mg normalized to cell number. $N = 3$, Mann–Whitney test. ****$p < .0001$. Data are the mean ± SEM. (ai) Representative images of senescence-associated beta galactosidase (SA-β-gal) staining in Dex and RU/Dex pre-treated iPS-Mg. (aii) SA-β-gal activity quantified by staining intensity in Dex or RU/Dex pre-treated iPS-Mg normalized to cell number. $N = 4$. Kruskal-Wallis test with Dunn's multiple comparison test. **$p < .01$. Data are the mean ± SEM. (b) Relative telomere length determined by real-time qPCR in NT, Dex and RU/Dex pre-treated iPS-Mg. NT-, and Dex-iPS-Mg, $N = 3$; RU/Dex-iPS-Mg, $N = 2$. (ci) Representative human XL cytokine proteome array dot blots from Dex and RU/Dex pre-treated. $N = 2$ membranes with 2–3 separate pooled replicates. (cii) Quantification of the expression of 11 Senescence-Associated Secretory Phenotype (SASP) related proteins. Expression level of SASP related proteins are normalized to NT iPS-Mg as basal secretion. Dex treated iPS-Mg has overarching higher expression of SASP related proteins. $N = 2$. Data are the mean ± SEM. Statistical significance was addressed using one way ANOVA with Dunnett's multiple comparison test, or Kruskal-Wallis test with Dunn's multiple comparison test to compare nontreated group with the Dex and RU/Dex treated group, *$P < .05$; **$P < .01$; ***$P < .005$

RU/Dex-iPS-Mg. We detected a significantly higher number of cGAS positive micronuclei in Dex-iPS-Mg compared with NT- iPS-Mg (Figure 5D), or RU/Dex-iPS-Mg.

3.7 | Proliferation inhibition and senescence features were present in Dex-iPS-Mg

One observation of GR activation was a significant reduction in the cell number of Dex-iPS-MPro compared with NT-iPS-MPro or RU/Dex-iPS-MPro (Figure 6a). This suggested that certain proliferation related processes or cellular components might be affected by Dex exposure. Thus, we revisited the GSEA analysis on the whole transcriptomics of NT and Dex-iPS-Mg, specifically focusing on the top 10 highest score of gene ratio among all other examined enriched pathways. Gene ratio is the percentage of total DEGs in the given GO term. We discovered that the condensin complex (cellular component, CC), mitotic spindle elongation and spindle midzone assembly (biological processes, BP) are all suppressed (Figure 6b, marked with ★). Taken together, suppressed genes of condensin complex and mitotic spindle elongation, and significantly reduced cell number in Dex-iPS-Mg suggests defective proliferation, and possibly cellular senescence.

The link between cGAS positive micronucleated cells and senescence is well established (Glück & Ablasser, 2019). Since Dex-iPS-Mg expressed an increase in the number of cGAS positive micronuclei, the microglia might also exhibit cellular senescence. As one characteristic of senescent cells is the loss of proliferative capacity (Galvis et al., 2019), we analyzed the expression of the proliferation marker, Ki67 in NT-Dex- and RU/Dex-iPS-Mg. Dex-iPS-Mg displayed a significantly reduced Ki67 expression compared with NT, and relatively lower expression of Ki67 compared with RU/Dex (Figure 6c).

We also examined changes to three "gold standard" senescence markers, namely, senescence- associated beta galactosidase (SA-β-gal), senescence-associated Secretory Phenotype (SASP), and relative telomere length (reviewed in Galvis et al., 2019). Dex treated iPS-Mg showed significantly greater intensity of SA-β-gal staining compared with NT or RU/Dex iPS-Mg (Figure 7a). In addition, Dex-iPS- Mg displayed a trend toward shorter telomere lengths compared with NT- iPS-Mg (Figure 7b). Furthermore, of 105 cytokines and chemokines investigated as secreted in conditioned medium, the most significantly upregulated were 11 SASP proteins previously shown to be upregulated in senescent cells (Lunyak et al., 2017) and here showed increased expression in Dex compared with NT or RU/Dex-iPS- Mg (Figure 7c). Taken together, we demonstrated here that in Dex-iPS-Mg, there is an overarching presence of senescent characteristics.

4 | DISCUSSION

Here, we demonstrate for the first time that human iPS-Mg express GR (NR3C1), and furthermore that this is the splice variant GR-α. This corresponds to the active form of the receptor, that is, one that can be activated by cortisol (Hagendorf et al., 2005). GR-α levels and activity are modulated by GR-β and GR-P isoforms (Hagendorf et al., 2005). We did not detect the expression of GR-β in our cells, either at the iPSC stage or following differentiation to microglia. Moreover, we also found that from the development of the iPSC to iPS-Mg, the expression of NR3C1 total, and NR3C1 1E increased, which reflect a development to a more specific immune phenotype. Previously Lieberman et al. (2017) demonstrated that GR mRNA expression levels increased during the differentiation of iPSC-derived neural cells; GR mRNA has also been shown to be increased in human iPS derived cerebral organoids (Cruceanu et al., 2022).

Meanwhile, our study is the first to show the young age verification of iPS-Mg, which motivates us to construct a cellular model correlates with ELS. Furthermore, we established an in vitro model of ELS in iPS-Mg mimicking prenatal exposure to GCs by prolonged activation of GR during 2nd stage of primitive haemotopoesis. By RNA-Seq analysis on iPS-Mg, we found continuous activation of GR during 2nd stage of primitive haemotopoesis triggered enhanced signaling of type I interferon, formation of cGAS positive micronuclei together with cellular senescence in the fully differentiated and maturated iPS-Mg. As we only modulated GR activation during primitive hematopoiesis before differentiation and maturation of iPS-Mg, what we observed and reported here is the priming effect and after-effect of aberrant GR activation during microglial development.

The GR expression and its related changes in iPSC and iPS-Mg provide a good platform for further investigation of GR function in microglial development. Specifically, the iPS-Mg model can be useful in understanding disease- and treatment-associated acquired GC resistance. Dex-iPS-Mg transcriptomics identified gene expression alterations related to psychiatric diseases. For example, our findings of elevated FKBP5 paralleled in vivo model of ELS (Ke et al., 2018), and FKBP5 overexpression related to aging and increased risks for several disorders, including depression (Binder et al., 2004; Ferrer et al., 2018; Menke et al., 2013; Zannas et al., 2019) and type 2 schizophrenic patients (Bowen et al., 2019). Meanwhile, Dex-iPS-Mg upregulates the microglial signature gene TMEM119, mimicking the effect observed in an in vivo ELS model (Ozaki et al., 2020). Clinically, similar increases in TMEM119 mRNA and protein were identified in post-mortem microglia from major depressive disorder patients (Böttcher et al., 2020; Snijders et al., 2021). Moreover, enhanced type I interferon signaling, which is enriched in Dex- and Cort-iPS-Mg and primary microglia from in vivo ELS model (Delpech et al., 2016), has the strongest association with recurrent major depressive patients (Mostafavi et al., 2014). Dex- and Cort- iPS-Mg reveals comparable molecular hallmarks of psychiatric illnesses; because our treatment paradigm correlates with ELS, it has applications to unravel molecular pathways underlying the developmental origins of psychiatric disease.

Here, we confirmed that one possible cause of increased type I interferon and viral defense signaling in Dex-iPS-Mg was more frequent micronuclei with activated cGAS. Cancer cells are well-known to acquire high number of cGAS positive micronuclei due to its inherent genomic instability (Gisselsson et al., 2001; Mackenzie

et al., 2017). However, recent evidence points to genomic instability and copy number variation in ASD and schizophrenia (Kushima et al., 2018). To our knowledge, this is first time that prolonged activation of GR during primitive hematopoiesis results in genomic instability and cellular senescence in the resultant microglia. This phenomenon of genomic instability shown here in human iPS-Mg is central to brain cell-specific involvement in ASD and schizophrenia because of the excessive GC exposure paradigm at an early stage of microglia development, which links to an ELS paradigm and is linked to ASD and schizophrenia.

Our finding that GR activation (by Dex) led to a reduction in cell number (of iPS-MPro) has been reported for other cell types (Piette et al., 2009; Samuelsson et al., 1999), where it reflected an inhibition of proliferation (Piette et al., 2009). In line with this, we report that proliferation (as measured by Ki67 expression) was reduced in the iPS-Mg following their early exposure to Dex at the iPS-MPro stage (suggesting a maintained phenotype effect). The loss of proliferative capacity in Dex iPS-Mg supports the senescence features we observed, which shows significant increased SA-β-gal activity, SASP and trend of shorter average relative telomere length. Additionally, WGCNA analysis validates our observed senescence features. Enrichment of macroautophagy and autophagy pathways correlates strongly with GR activation, as being reflected by enhanced lysosomal SA-β-gal activity in Dex-iPS-Mg. Our senescence finding matches earlier research. Senescence and autophagy activation is specific to Dex treatment in primary rodent microglia (Park et al., 2019), and cGAS-STING signaling (Hopfner & Hornung, 2020). Surprisingly, major depression is linked with enhanced molecular senescence abnormalities (higher SASP in serum) (Diniz et al., 2019), and dysregulated GC has been implicated in depression and ELS (Anacker et al., 2011; Gotlib et al., 2021). Altogether, our in vitro ELS model has implications for microglia responses in GC-mediated ELS-associated diseases such as depression, schizophrenia, ADHD, and ASD.

ELS-mediated high GC may result in chronic occupancy of GRs' ligand-binding region, which may explain our ELS treatment paradigm-induced phenotype. This reduces vacant GRs and impairs the accuracy of chromosome segregation. GRs regulate accurate chromosomal segregation. As Matthews et al. (2015) noted that unliganded (free) GRs' ligand-binding domain regulates mitotic spindle function. This is consistent with our discovery of more micronuclei in Dex-iPS-Mg and fewer in RU/Dex-iPS-Mg. Our discovery contrasts with the anti-inflammatory and immunosuppressive effects of acute GC therapy, where GCs decrease type I interferon signaling (Flammer et al., 2010). Our results add to the intriguing consequences associated with excessive GCs in the context of microglial development.

One strength of current study is that we utilized a Dex concentration of 50 nM, which is sub- therapeutic and within a physiological relevant range (Jameson et al., 2006); human preterm infants typically receive 0.1–0.15 mg/kg Dex, which is about 0.6 μM when given directly to a preterm infant, or 0.06 μM in the fetus when Dex is given to the mother (Charles et al., 1993; Osathanondh et al., 1977). The use of the endogenous GR activator, hydrocortisone (Cort), at a comparative concentration to Dex treatment (Longui et al., 2005), confirmed the findings of the synthetic agonist.

Previous studies only captured the immediate effect of ELS on embryonic or early postnatal microglia following short ELS exposures. Thus, prenatal increased GC was revealed to increase overall microglial density and promote an immunoreactive embryonic microglial phenotype after brief 2 days ELS exposure (Bittle & Stevens, 2018) which differs from our findings. 72-hr aberrant GR stimulation in early postnatal rat primary microglia downregulates CX3CR1 and TREM2 and induces senescence (Park et al., 2019). Our work provides insight into the priming effect of early chronically activated GR on subsequent microglia development.

ELS via GR activation on microglia has mostly been studied in rodents. Humans and animal models have varied immunological responses, and experimental rodents are reared in contained environments during early development, and exhibit life-span differences (Smith & Dragunow, 2014). Thus, it has proven difficult to translate findings from rodent microglia to human microglia. Given these caveats, the current model can provide an alternative model for manipulation at an early developmental stage which has an impact on subsequent microglial phenotypes. Particularly, the WGCNA analysis suggests histone and chromatin modification in our ELS iPS-Mg. Consistent with this, it is well known that epigenetic modifications and reprogramming are associated with the consequences and effect of ELS (Krontira et al., 2020; Weaver et al., 2014).

Currently, our study has some limitations. In the absence of data from post-mortem tissues or co-culturing with other brain cell types and functional investigations such as electrophysiology, our results should not be extrapolated to a unified explanation of the etiology of ELS-associated disorders. Meanwhile, we established a model of GC activation in microglia and, using the excessive exposure paradigm at an early stage of microglial development links/correlates the model to an ELS paradigm. Thus, our current findings only imply the consequences of early GC activation-mediated ELS-associated disorder in microglia rather than all ELS-associated disorders. Although the influence of dysregulated prenatal GC (endogenous GC, (Rim et al., 2022)); (exogenous GC, (Block et al., 2022)) on microglia function and depressive-like and schizophrenic-like behaviors have been directly linked in recent in vivo studies, it is unclear whether this is a primary or secondary cause of these disorders.

5 | CONCLUSIONS

In summary, we have established that an in vitro model of GC-mediated ELS in iPS-Mg can induce certain biological consequences of ELS found in vivo. We found that prolonged activation of GR during microglial development led to genomic instability via frequent formation of cGAS-positive micronucleus and complemented with cellular senescence. GC-mediated ELS-related epigenetic alteration and reprogramming could be further investigated using our model. These data have ramifications for developmental conditions following maternal GC stress.

AUTHOR CONTRIBUTIONS

Jingzhang Wei and Thomas M Piers devised the project with input from Jennifer M Pocock. Jingzhang Wei carried out all the experiments. The pathway enrichment analysis was done by Thomas M Piers. Charles Arber assisted with the qPCR, Jingzhang Wei and Jennifer M Pocock wrote the paper. All authors reviewed the paper.

ACKNOWLEDGMENTS

The running costs for the project were provided by J.M.P and J.H. Additional funding for the RNA-seq analysis was provided to J.W., T.M.P. and J.M.P. with a pump-priming grant from the Alzheimer's Research UK. This research used the UCL genomics facilities and UCL Cancer Institute sequencing facilities. C.A. was supported by a fellowship from the Alzheimer's Society UK (AS-JF-18-008) in the lab of S.W. who was supported by an Alzheimer's Research UK Senior Research Fellowship (ARUK- SRF2016B-2) and the National Institute for Health Research University College London Hospitals Biomedical Research Centre. We acknowledge access to the database of Genotypes and Phenotypes (dbGaP) for datasets on young microglia (Gosselin et al., 2017), mid-age microglia (Zhang et al., 2016), and SYNAPSE (Olah et al., 2018) for datasets on old microglia, and all age microglia (Galatro et al., 2017).

CONFLICT OF INTEREST

The authors declare no conflicts of interest.

DATA AVAILABILITY STATEMENT

Accession codes: Gene Expression Omnibus GSE73721 (Zhang et al., 2016), GSE99074 (Galatro et al., 2017), dbGaP: phs001373.v2.p2 (Gosselin et al., 2017), SYNAPSE: syn3219045, syn11468526 (Olah et al., 2018).Our RNA-Seq data is available on request.

ORCID

Jennifer M. Pocock https://orcid.org/0000-0001-5812-9331

REFERENCES

Abud, E. M., Ramirez, R. N., Martinez, E. S., Healy, L. M., Nguyen, C. H. H., Newman, S. A., Yeromin, A. V., Scarfone, V. M., Marsh, S. E., Fimbres, C., Caraway, C. A., Fote, G. M., Madany, A. M., Agrawal, A., Kayed, R., Gylys, K. H., Cahalan, M. D., Cummings, B. J., Antel, J. P., … Blurton-Jones, M. (2017). iPSC-derived human microglia-like cells to study neurological diseases. *Neuron*, *94*(2), 278–293.e9.

Anacker, C., Zunszain, P. A., Carvalho, L. A., & Pariante, C. M. (2011). The glucocorticoid receptor: Pivot of depression and of antidepressant treatment? *Psychoneuroendocrinology*, *36*(3), 415–425.

Attardi, B. J., Burgenson, J., Hild, S. A., & Reel, J. R. (2004). In vitro antiprogestational/antiglucocorticoid activity and progestin and glucocorticoid receptor binding of the putative metabolites and synthetic derivatives of CDB-2914, CDB-4124, and mifepristone. *The Journal of Steroid Biochemistry and Molecular Biology*, *88*(3), 277–288.

Baquedano, E., García-Cáceres, C., Diz-Chaves, Y., Lagunas, N., Calmarza-Font, I., Azcoitia, I., Garcia-Segura, L. M., Argente, J., Chowen, J. A., & Frago, L. M. (2011). Prenatal stress induces long-term effects in cell turnover in the hippocampus-hypothalamus-pituitary axis in adult male rats. *PLoS One*, *6*(11), e27549.

Barbazanges, A., Piazza, P. V., Le Moal, M., & Maccari, S. (1996). Maternal glucocorticoid secretion mediates long-term effects of prenatal stress. *The Journal of Neuroscience*, *16*(12), 3943–3949.

Benediktsson, R., Lindsay, R. S., Noble, J., Seckl, J. R., & Edwards, C. R. (1993). Glucocorticoid exposure in utero: New model for adult hypertension. *Lancet*, *341*(8841), 339–341.

Binder, E. B. (2009). The role of FKBP5, a co-chaperone of the glucocorticoid receptor in the pathogenesis and therapy of affective and anxiety disorders. *Psychoneuroendocrinology*, *34*-(Suppl 1), S186–S195.

Binder, E. B., Salyakina, D., Lichtner, P., Wochnik, G. M., Ising, M., Pütz, B., Papiol, S., Seaman, S., Lucae, S., Kohli, M. A., Nickel, T., Künzel, H. E., Fuchs, B., Majer, M., Pfennig, A., Kern, N., Brunner, J., Modell, S., Baghai, T., … Muller-Myhsok, B. (2004). Polymorphisms in FKBP5 are associated with increased recurrence of depressive episodes and rapid response to antidepressant treatment. *Nature Genetics*, *36*(12), 1319–1325.

Bittle, J., & Stevens, H. E. (2018). The role of glucocorticoid, interleukin-1β, and antioxidants in prenatal stress effects on embryonic microglia. *Journal of Neuroinflammation*, *15*(1), 44.

Block, C. L., Eroglu, O., Mague, S. D., Smith, C. J., Ceasrine, A. M., Sriworarat, C., Blount, C., Beben, K. A., Malacon, K. E., Ndubuizu, N., Talbot, A., Gallagher, N. M., Jo, Y. C., Nyangacha, T., Carlson, D. E., Dzirasa, K., Eroglu, C., & Bilbo, S. D. (2022). Prenatal environmental stressors impair postnatal microglia function and adult behavior in males. *Cell Reports*, *40*(5), 111161.

Böttcher, C., Fernández-Zapata, C., Snijders, G. J. L., Schlickeiser, S., Sneeboer, M. A. M., Kunkel, D., de Witte, L. D., & Priller, J. (2020). Single-cell mass cytometry of microglia in major depressive disorder reveals a non-inflammatory phenotype with increased homeostatic marker expression. *Translational Psychiatry*, *10*, 310.

Bowen, E. F., Burgess, J. L., Granger, R., Kleinman, J. E., & Rhodes, C. H. (2019). DLPFC transcriptome defines two molecular subtypes of schizophrenia. *Translational Psychiatry*, *9*(1), 1–10.

Buss, C., Davis, E. P., Shahbaba, B., Pruessner, J. C., Head, K., & Sandman, C. A. (2012). Maternal cortisol over the course of pregnancy and subsequent child amygdala and hippocampus volumes and affective problems. *Proceedings of the National Academy of Sciences*, *109*(20), E1312–E1319.

Cawthon, R. M. (2002). Telomere measurement by quantitative PCR. *Nucleic Acids Research*, *30*(10), e47.

Charles, B., Schild, P., Steer, P., Cartwright, D., & Donovan, T. (1993). Pharmacokinetics of dexamethasone following single-dose intravenous administration to extremely low birth weight infants. *Developmental Pharmacology and Therapeutics*, *20*(3–4), 205–210.

Chen, W., Liu, N., Shen, S., Zhu, W., Qiao, J., Chang, S., Dong, J., Bai, M., Ma, L., Wang, S., Jia, W., Guo, X., Li, A., Xi, J., Jiang, C., & Kang, J. (2021). Fetal growth restriction impairs hippocampal neurogenesis and cognition via Tet1 in offspring. *Cell Reports*, *37*(5), 109912.

Cosker, K., Mallach, A., Limaye, J., Piers, T. M., Staddon, J., Neame, S. J., Hardy, J., & Pocock, J. M. (2021). Microglial signalling pathway deficits associated with the patient derived R47H TREM2 variants linked to AD indicate inability to activate inflammasome. *Scientific Reports*, *11*(1), 13316.

Courchesne, E., Gazestani, V. H., & Lewis, N. E. (2020). Prenatal origins of ASD: The when, what, and how of ASD development. *Trends in Neurosciences*, *43*(5), 326–342.

Cruceanu, C., Dony, L., Krontira, A. C., Fischer, D. S., Roeh, S., Di Giaimo, R., Kyrousi, C., Kaspar, L., Arloth, J., Czamara, D., Gerstner, N., Martinelli, S., Wehner, S., Breen, M. S., Koedel, M., Sauer, S., Sportelli, V., Rex-Haffner, M., Cappello, S., … Binder, E. B. (2022). Cell-type- specific impact of glucocorticoid receptor activation on the developing brain: A cerebral organoid study. *The American Journal of Psychiatry*, *179*(5), 375–387.

Cunningham, C. L., Martínez-Cerdeño, V., & Noctor, S. C. (2013). Microglia regulate the number of neural precursor cells in the developing cerebral cortex. *The Journal of Neuroscience*, *33*(10), 4216–4233.

Davenport, C. M., Sevastou, I. G., Hooper, C., & Pocock, J. M. (2010). Inhibiting p53 pathways in microglia attenuates microglial-evoked neurotoxicity following exposure to Alzheimer peptides. *Journal of Neurochemistry*, *112*(2), 552–563.

Davis, E. P., Sandman, C. A., Buss, C., Wing, D. A., & Head, K. (2013). Fetal glucocorticoid exposure is associated with preadolescent brain development. *Biological Psychiatry*, *74*(9), 647–655.

Davis, E. P., Waffarn, F., & Sandman, C. A. (2011). Prenatal treatment with glucocorticoids sensitizes the hpa axis response to stress among full-term infants. *Developmental Psychobiology*, *53*(2), 175–183.

de la Fuente, A. (2010). From 'differential expression' to 'differential networking' - identification of dysfunctional regulatory networks in diseases. *Trends in Genetics*, *26*(7), 326–333.

Delpech, J. C., Wei, L., Hao, J., Yu, X., Madore, C., Butovsky, O., & Kaffman, A. (2016). Early life stress perturbs the maturation of microglia in the developing hippocampus. *Brain, Behavior, and Immunity*, *57*, 79–93.

Diniz, B. S., Reynolds Iii, C. F., Sibille, E., Bot, M., & Penninx, B. W. J. H. (2019). Major depression and enhanced molecular senescence abnormalities in young and middle-aged adults. *Translational Psychiatry*, *9*(1), 198.

Dubik, N., & Mai, S. (2020). Lamin A/C: Function in normal and tumor cells. *Cancers (Basel)*, *12*(12), 3688. doi:10.3390/cancers12123688

Faresjö, T., Strömberg, S., Jones, M., Stomby, A., Karlsson, J. E., Östgren, C. J., Faresjö, Å., & Theodorsson, E. (2020). Elevated levels of cortisol in hair precede acute myocardial infarction. *Scientific Reports*, *10*, 22456.

Ferrer, A., Costas, J., Labad, J., Salvat-Pujol, N., Segalàs, C., Urretavizcaya, M., Real, E., de Arriba- Arnau, A., Alonso, P., Crespo, J. M., Barrachina, M., Soriano-Mas, C., Carracedo, Á., Menchón, J. M., & Soria, V. (2018). FKBP5 polymorphisms and hypothalamic-pituitary-adrenal axis negative feedback in major depression and obsessive-compulsive disorder. *Journal of Psychiatric Research*, *104*, 227–234.

Flammer, J. R., Dobrovolna, J., Kennedy, M. A., Chinenov, Y., Glass, C. K., Ivashkiv, L. B., & Rogatsky, I. (2010). The type I interferon signaling pathway is a target for glucocorticoid inhibition. *Molecular and Cellular Biology*, *30*(19), 4564–4574.

Fujioka, T., Sakata, Y., Yamaguchi, K., Shibasaki, T., Kato, H., & Nakamura, S. (1999). The effects of prenatal stress on the development of hypothalamic paraventricular neurons in fetal rats. *Neuroscience*, *92*, 1079–1088.

Fukumoto, K., Morita, T., Mayanagi, T., Tanokashira, D., Yoshida, T., Sakai, A., & Sobue, K. (2009). Detrimental effects of glucocorticoids on neuronal migration during brain development. *Molecular Psychiatry*, *14*(12), 1119–1131.

Galatro, T. F., Holtman, I. R., Lerario, A. M., Vainchtein, I. D., Brouwer, N., Sola, P. R., Veras, M. M., Pereira, T. F., Leite, R. E. P., Möller, T., Wes, P. D., Sogayar, M. C., Laman, J. D., den Dunnen, W., Pasqualucci, C. A., Oba-Shinjo, S. M., Boddeke, E. W. G. M., Marie, S. K. N., & Eggen, B. J. L. (2017). Transcriptomic analysis of purified human cortical microglia reveals age-associated changes. *Nature Neuroscience*, *20*(8), 1162–1171.

Galvis, D., Walsh, D., Harries, L. W., Latorre, E., & Rankin, J. (2019). A dynamical systems model for the measurement of cellular senescence. *Journal of the Royal Society Interface*, *16*(159), 20190311.

Garcia-Reitboeck, P., Phillips, A., Piers, T. M., Villegas-Llerena, C., Butler, M., Mallach, A., Rodrigues, C., Arber, C. E., Heslegrave, A., Zetterberg, H., Neumann, H., Neame, S., Houlden, H., Hardy, J., & Pocock, J. M. (2018). Human induced pluripotent stem cell-derived microglia-like cells harboring TREM2 missense mutations show specific deficits in phagocytosis. *Cell Reports*, *24*(9), 2300–2311.

Ginhoux, F., Greter, M., Leboeuf, M., Nandi, S., See, P., Gokhan, S., Mehler, M. F., Conway, S. J., Ng, L. G., Stanley, E. R., Samokhvalov, I. M., & Merad, M. (2010). Fate mapping analysis reveals that adult microglia derive from primitive macrophages. *Science*, *330*(6005), 841–845.

Gisselsson, D., Björk, J., Höglund, M., Mertens, F., Dal Cin, P., Akerman, M., & Mandahl, N. (2001). Abnormal nuclear shape in solid tumors reflects mitotic instability. *The American Journal of Pathology*, *158*(1), 199–206.

Glück, S., & Ablasser, A. (2019). Innate immunosensing of DNA in cellular senescence. *Current Opinion in Immunology*, *56*, 31–36.

Gosselin, D., Skola, D., Coufal, N. G., Holtman, I. R., Schlachetzki, J. C. M., Sajti, E., Jaeger, B. N., O'Connor, C., Fitzpatrick, C., Pasillas, M. P., Pena, M., Adair, A., Gonda, D. D., Levy, M. L., Ransohoff, R. M., Gage, F. H., & Glass, C. K. (2017). An environment-dependent transcriptional network specifies human microglia identity. *Science*, *356* (6344), eaal3222.

Gotlib, I. H., Borchers, L. R., Chahal, R., Gifuni, A. J., Teresi, G. I., & Ho, T. C. (2021). Early life stress predicts depressive symptoms in adolescents during the COVID-19 pandemic: The mediating role of perceived stress. *Frontiers in Psychology*, *11*, 3864.

Guess, A., Agrawal, S., Wei, C. C., Ransom, R. F., Benndorf, R., & Smoyer, W. E. (2010). Dose- and time-dependent glucocorticoid receptor signaling in podocytes. *American Journal of Physiology. Renal Physiology*, *299*(4), F845–F853.

Haenseler, W., Sansom, S. N., Buchrieser, J., Newey, S. E., Moore, C. S., Nicholls, F. J., Chintawar, S., Schnell, C., Antel, J. P., Allen, N. D., Cader, M. Z., Wade-Martins, R., James, W. S., & Cowley, S. A. (2017). A highly efficient human pluripotent stem cell microglia model displays a neuronal- co-culture-specific expression profile and inflammatory response. *Stem Cell Reports*, *8*(6), 1727–1742.

Hagendorf, A., Koper, J. W., de Jong, F. H., Brinkmann, A. O., Lamberts, S. W., & Feelders, R. A. (2005). Expression of the human glucocorticoid receptor splice variants alpha, beta, and P in peripheral blood mononuclear leukocytes in healthy controls and in patients with hyper- and hypocortisolism. *The Journal of Clinical Endocrinology and Metabolism*, *90*(11), 6237–6243.

Harris, A., & Seckl, J. (2011). Glucocorticoids, prenatal stress and the programming of disease. *Hormones and Behavior*, *59*(3), 279–289.

Hatch, E. M., Fischer, A. H., Deerinck, T. J., & Hetzer, M. W. (2013). Catastrophic nuclear envelope collapse in cancer cell micronuclei. *Cell*, *154*(1), 47–60.

Heard, K. J., Shokhirev, M. N., Becronis, C., Fredlender, C., Zhaid, N., Le, A. T., Ji, Y., Skime, M., Nelson, T., Hall-Flavin, D., Weinshilboum, R., Gage, F. H., & Vadodaria, K. C. (2021). Chronic cortisol differentially impacts stem cell-derived astrocytes from major depressive disorder patients. *Translational Psychiatry*, *11*, 608.

Honda, K., Takaoka, A., & Taniguchi, T. (2006). Type I interferon [corrected] gene induction by the interferon regulatory factor family of transcription factors. *Immunity*, *25*(3), 349–360.

Hopfner, K. P., & Hornung, V. (2020). Molecular mechanisms and cellular functions of cGAS- STING signalling. *Nature Reviews. Molecular Cell Biology*, *21*(9), 501–521.

Jameson, R. R., Seidler, F. J., Qiao, D., & Slotkin, T. A. (2006). Adverse neurodevelopmental effects of dexamethasone modeled in PC12 cells: Identifying the critical stages and concentration thresholds for the targeting of cell acquisition, differentiation and viability. *Neuropsychopharmacology*, *31*(8), 1647–1658.

Joglekar, M. V., Satoor, S. N., Wong, W. K. M., Cheng, F., Ma, R. C. W., & Hardikar, A. A. (2020). An optimised step-by-step protocol for measuring relative telomere length. *Methods and Protocols*, *3*(2), 27.

Joseph, J. J., & Golden, S. H. (2017). Cortisol dysregulation: The bidirectional link between stress, depression, and type 2 diabetes mellitus. *Annals of the New York Academy of Sciences*, *1391*(1), 20–34.

Ke, X., Fu, Q., Majnik, A., Cohen, S., Liu, Q., & Lane, R. (2018). Adverse early life environment induces anxiety-like behavior and increases expression of FKBP5 mRNA splice variants in mouse brain. *Physiological Genomics*, *50*(11), 973–981.

Keating, S. E., Baran, M., & Bowie, A. G. (2011). Cytosolic DNA sensors regulating type I interferon induction. *Trends in Immunology*, *32*(12), 574–581.

Kim, D., Paggi, J. M., Park, C., Bennett, C., & Salzberg, S. L. (2019). Graph-based genome alignment and genotyping with HISAT2 and HISAT-genotype. *Nature Biotechnology*, *37*(8), 907–915.

Kneissig, M., Keuper, K., de Pagter, M. S., van Roosmalen, M. J., Martin, J., Otto, H., Passerini, V., Campos Sparr, A., Renkens, I., Kropveld, F., Vasudevan, A., Sheltzer, J. M., Kloosterman, W. P., & Storchova, Z. (2019). Micronuclei-based model system reveals functional consequences of chromothripsis in human cells. *eLife*, *8*, e50292.

Krontira, A. C., Cruceanu, C., & Binder, E. B. (2020). Glucocorticoids as mediators of adverse outcomes of prenatal stress. *Trends in Neurosciences*, *43*(6), 394–405.

Kushima, I., Aleksic, B., Nakatochi, M., Shimamura, T., Okada, T., Uno, Y., Morikawa, M., Ishizuka, K., Shiino, T., Kimura, H., Arioka, Y., Yoshimi, A., Takasaki, Y., Yu, Y., Nakamura, Y., Yamamoto, M., Iidaka, T., Iritani, S., Inada, T., … Ozaki, N. (2018). Comparative analyses of copy-number variation in autism spectrum disorder and schizophrenia reveal etiological overlap and biological insights. *Cell Reports*, *24*(11), 2838–2856.

Kwon, M., Leibowitz, M. L., & Lee, J. H. (2020). Small but mighty: The causes and consequences of micronucleus rupture. *Experimental & Molecular Medicine*, *52*(11), 1777–1786.

Langfelder, P., & Horvath, S. (2008). WGCNA: An R package for weighted correlation network analysis. *BMC Bioinformatics*, *9*(1), 559.

Langfelder, P., Luo, R., Oldham, M. C., & Horvath, S. (2011). Is my network module preserved and reproducible? *PLoS Computational Biology*, *7*(1), e1001057.

Liao, Y., Smyth, G. K., & Shi, W. (2014). featureCounts: An efficient general purpose program for assigning sequence reads to genomic features. *Bioinformatics*, *30*(7), 923–930.

Liao, Y., Smyth, G. K., & Shi, W. (2019). The R package Rsubread is easier, faster, cheaper and better for alignment and quantification of RNA sequencing reads. *Nucleic Acids Research*, *47*(8), e47.

Lieberman, R., Kranzler, H. R., Levine, E. S., & Covault, J. (2017). Examining FKBP5 mRNA expression in human iPSC-derived neural cells. *Psychiatry Research*, *247*, 172–181.

Liu, L., Aleksandrowicz, E., Schönsiegel, F., Gröner, D., Bauer, N., Nwaeburu, C. C., Zhao, Z., Gladkich, J., Hoppe-Tichy, T., Yefenof, E., Hackert, T., Strobel, O., & Herr, I. (2017). Dexamethasone mediates pancreatic cancer progression by glucocorticoid receptor, TGFβ and JNK/AP-1. *Cell Death & Disease*, *8*(10), e3064.

Longui, C. A., Santos, M. C., Formiga, C. B., Oliveira, D. V., Rocha, M. N., Faria, C. D., Kochi, C., & Monte, O. (2005). Antiproliferative and apoptotic potencies of glucocorticoids: Nonconcordance with their antiinflammatory and immunosuppressive properties. *Arquivos Brasileiros de Endocrinologia e Metabologia*, *49*(3), 378–383.

Love, M. I., Huber, W., & Anders, S. (2014). Moderated estimation of fold change and dispersion for RNA-seq data with DESeq2. *Genome Biology*, *15*(12), 550.

Lu, N. Z., & Cidlowski, J. A. (2005). Translational regulatory mechanisms generate N-terminal glucocorticoid receptor isoforms with unique transcriptional target genes. *Molecular Cell*, *18*(3), 331–342.

Lunyak, V. V., Amaro-Ortiz, A., & Gaur, M. (2017). Mesenchymal stem cells secretory responses: Senescence messaging secretome and immunomodulation perspective. *Frontiers in Genetics*, *8*, 220.

Lupien, S. J., McEwen, B. S., Gunnar, M. R., & Heim, C. (2009). Effects of stress throughout the lifespan on the brain, behaviour and cognition. *Nature Reviews. Neuroscience*, *10*(6), 434–445.

Mackenzie, K. J., Carroll, P., Martin, C.-A., Murina, O., Fluteau, A., Simpson, D. J., Olova, N., Sutcliffe, H., Rainger, J. K., Leitch, A., Osborn, R. T., Wheeler, A. P., Nowotny, M., Gilbert, N., Chandra, T., Reijns, M. A. M., & Jackson, A. P. (2017). cGAS surveillance of micronuclei links genome instability to innate immunity. *Nature*, *548*(7668), 461–465.

Mallach, A., Gobom, J., Arber, C., Piers, T. M., Hardy, J., Wray, S., Zetterberg, H., & Pocock, J. (2021). Differential stimulation of pluripotent stem cell-derived human microglia leads to exosomal proteomic changes affecting neurons. *Cells*, *10*(11), 2866.

Manzari, N., Matvienko-Sikar, K., Baldoni, F., O'Keeffe, G. W., & Khashan, A. S. (2019). Prenatal maternal stress and risk of neurodevelopmental disorders in the offspring: A systematic review and meta-analysis. *Social Psychiatry and Psychiatric Epidemiology*, *54*(11), 1299–1309.

Matthews, L. C., Berry, A. A., Morgan, D. J., Poolman, T. M., Bauer, K., Kramer, F., Spiller, D. G., Richardson, R. V., Chapman, K. E., Farrow, S. N., Norman, M. R., Williamson, A. J., Whetton, A. D., Taylor, S. S., Tuckermann, J. P., White, M. R., & Ray, D. W. (2015). Glucocorticoid receptor regulates accurate chromosome segregation and is associated with malignancy. *Proceedings of the National Academy of Sciences of the United States of America*, *112*(17), 5479–5484.

Menke, A., Klengel, T., Rubel, J., Brückl, T., Pfister, H., Lucae, S., Uhr, M., Holsboer, F., & Binder, E. B. (2013). Genetic variation in FKBP5 associated with the extent of stress hormone dysregulation in major depression. *Genes, Brain and Behavior*, *12*(3), 289–296.

Middlebrooks, J. S., & Audage, N. C. (2008). The effects of childhood stress on health across the lifespan. National Center for Injury Prevention and Control of the Centers for Disease Control and Prevention.

Miller, K. N., Victorelli, S. G., Salmonowicz, H., Dasgupta, N., Liu, T., Passos, J. F., & Adams, P. D. (2021). Cytoplasmic DNA: Sources, sensing, and role in aging and disease. *Cell*, *184*(22), 5506–5526.

Mondelli, V., Vernon, A. C., Turkheimer, F., Dazzan, P., & Pariante, C. M. (2017). Brain microglia in psychiatric disorders. *Lancet Psychiatry*, *4*(7), 563–572.

Monier, A., Adle-Biassette, H., Delezoide, A. L., Evrard, P., Gressens, P., & Verney, C. (2007). Entry and distribution of microglial cells in human embryonic and fetal cerebral cortex. *Journal of Neuropathology and Experimental Neurology*, *66*(5), 372–382.

Moog, N. K., Entringer, S., Rasmussen, J. M., Styner, M., Gilmore, J. H., Kathmann, N., Heim, C. M., Wadhwa, P. D., & Buss, C. (2018). Intergenerational effect of maternal exposure to childhood maltreatment on newborn brain anatomy. *Biological Psychiatry*, *83*(2), 120–127.

Mostafavi, S., Battle, A., Zhu, X., Potash, J. B., Weissman, M. M., Shi, J., Beckman, K., Haudenschild, C., McCormick, C., Mei, R., Gameroff, M. J., Gindes, H., Adams, P., Goes, F. S., Mondimore, F. M., MacKinnon, D. F., Notes, L., Schweizer, B., Furman, D., … Levinson, D. F. (2014). Type I interferon signaling genes in recurrent major depression: Increased expression detected by whole-blood RNA sequencing. *Molecular Psychiatry*, *19*, 1267–1274.

Norppa, H., & Falck, G. C. (2003). What do human micronuclei contain? *Mutagenesis*, *18*(3), 221–233.

Nürnberg, E., Horschitz, S., Schloss, P., & Meyer-Lindenberg, A. (2018). Basal glucocorticoid receptor activation induces proliferation and inhibits neuronal differentiation of human induced pluripotent stem cell-derived neuronal precursor cells. *The Journal of Steroid Biochemistry and Molecular Biology*, *182*, 119–126.

Olah, M., Patrick, E., Villani, A.-C., Xu, J., White, C. C., Ryan, K. J., Piehowski, P., Kapasi, A., Nejad, P., Cimpean, M., Connor, S., Yung, C. J., Frangieh, M., McHenry, A., Elyaman, W., Petyuk, V., Schneider, J. A., Bennett, D. A., De Jager, P. L., & Bradshaw, E. M. (2018). A transcriptomic atlas of aged human microglia. *Nature Communications*, *9*(1), 539.

Osathanondh, R., Tulchinsky, D., Kamali, H., Fencl, M., & Taeusch, H. W., Jr. (1977). Dexamethasone levels in treated pregnant women and newborn infants. *The Journal of Pediatrics*, *90*(4), 617–620.

Ozaki, K., Kato, D., Ikegami, A., Hashimoto, A., Sugio, S., Guo, Z., Shibushita, M., Tatematsu, T., Haruwaka, K., Moorhouse, A. J., Yamada, H., & Wake, H. (2020). Maternal immune activation induces sustained changes in fetal microglia motility. *Scientific Reports*, *10*(1), 21378.

Park, M. J., Park, H. S., You, M. J., Yoo, J., Kim, S. H., & Kwon, M. S. (2019). Dexamethasone induces a specific form of ramified dysfunctional microglia. *Molecular Neurobiology*, *56*(2), 1421–1436.

Piers, T. M., Cosker, K., Mallach, A., Johnson, G. T., Guerreiro, R., Hardy, J., & Pocock, J. M. (2020). A locked immunometabolic switch underlies TREM2 R47H loss of function in human iPSC- derived microglia. *The FASEB Journal*, *34*(2), 2436–2450.

Piette, C., Deprez, M., Roger, T., Noël, A., Foidart, J. M., & Munaut, C. (2009). The dexamethasone-induced inhibition of proliferation, migration, and invasion in glioma cell lines is antagonized by macrophage migration inhibitory factor (MIF) and can be enhanced by specific MIF inhibitors. *The Journal of Biological Chemistry*, *284*(47), 32483–32492.

Provençal, N., Arloth, J., Cattaneo, A., Anacker, C., Cattane, N., Wiechmann, T., Röh, S., Ködel, M., Klengel, T., Czamara, D., Müller, N. S., Lahti, J., PREDO team, Räikkönen, K., Pariante, C. M., & Binder, E. B. (2020). Glucocorticoid exposure during hippocampal neurogenesis primes future stress response by inducing changes in DNA methylation. *Proceedings of the National Academy of Sciences*, *117*(38), 23280–23285.

Quinn, M. A., McCalla, A., He, B., Xu, X., & Cidlowski, J. A. (2019). Silencing of maternal hepatic glucocorticoid receptor is essential for normal fetal development in mice. *Communications Biology*, *2*(1), 104.

Rim, C., Park, H. S., You, M. J., Yang, B., Kim, H. J., Sung, S., & Kwon, M. S. (2022). Microglia involvement in sex-dependent behaviors and schizophrenia occurrence in offspring with maternal dexamethasone exposure. *Schizophrenia (Heidelb).*, *8*(1), 71.

Samuelsson, M. K., Pazirandeh, A., Davani, B., & Okret, S. (1999). p57Kip2, a glucocorticoid- induced inhibitor of cell cycle progression in HeLa cells. *Molecular Endocrinology*, *13*(11), 1811–1822.

Schafer, D. P., Lehrman, E. K., Kautzman, A. G., Koyama, R., Mardinly, A. R., Yamasaki, R., Ransohoff, R. M., Greenberg, M. E., Barres, B. A., & Stevens, B. (2012). Microglia sculpt postnatal neural circuits in an activity and complement-dependent manner. *Neuron*, *74*(4), 691–705.

Singer, G. A., Lloyd, A. T., Huminiecki, L. B., & Wolfe, K. H. (2005). Clusters of co-expressed genes in mammalian genomes are conserved by natural selection. *Molecular Biology and Evolution*, *22*(3), 767–775.

Smith, A. M., & Dragunow, M. (2014). The human side of microglia. *Trends in Neurosciences*, *37*(3), 125–135.

Smith, S. M., & Vale, W. W. (2006). The role of the hypothalamic-pituitary-adrenal axis in neuroendocrine responses to stress. *Dialogues in Clinical Neuroscience*, *8*(4), 383–395.

Snijders, G. J. L. J., Sneeboer, M. A. M., Fernández-Andreu, A., Udine, E., Boks, M. P., Ormel, P. R., van Berlekom, A. B., van Mierlo, H. C., Böttcher, C., Priller, J., Raj, T., Hol, E. M., Kahn, R. S., de Witte, L. D., & B. Psychiatric donor program of the Netherlands Brain. (2021). Distinct non-inflammatory signature of microglia in post-mortem brain tissue of patients with major depressive disorder. *Molecular Psychiatry*, *26*(7), 3336–3349.

Song, X., Ma, F., & Herrup, K. (2019). Accumulation of cytoplasmic DNA due to ATM deficiency activates the microglial viral response system with neurotoxic consequences. *The Journal of Neuroscience*, *39*(32), 6378–6394.

Squarzoni, P., Oller, G., Hoeffel, G., Pont-Lezica, L., Rostaing, P., Low, D., Bessis, A., Ginhoux, F., & Garel, S. (2014). Microglia modulate wiring of the embryonic forebrain. *Cell Reports*, *8*(5), 1271–1279.

Swanson, A. M., & David, A. L. (2015). Animal models of fetal growth restriction: Considerations for translational medicine. *Placenta*, *36*(6), 623–630.

Tijsseling, D., Wijnberger, L. D. E., Derks, J. B., van Velthoven, C. T. J., de Vries, W. B., van Bel, F., Nikkels, P. G. J., & Visser, G. H. A. (2012). Effects of antenatal glucocorticoid therapy on hippocampal histology of preterm infants. *PLoS One*, *7*(3), e33369.

Timmermans, S., Souffriau, J., & Libert, C. (2019). A general introduction to glucocorticoid biology. *Frontiers in Immunology*, *10*, 1545.

Turner, J. D., & Muller, C. P. (2005). Structure of the glucocorticoid receptor (NR3C1) gene 5′ untranslated region: Identification, and tissue distribution of multiple new human exon 1. *Journal of Molecular Endocrinology*, *35*(2), 283–292.

Vasilishina, A., Kropotov, A., Spivak, I., & Bernadotte, A. (2019). Relative human telomere length quantification by real-time PCR. *Methods in Molecular Biology*, *1896*, 39–44.

Weaver, I. C., Cervoni, N., Champagne, F. A., D'Alessio, A. C., Sharma, S., Seckl, J. R., Dymov, S., Szyf, M., & Meaney, M. J. (2014). Epigenetic programming by maternal behavior. *Nature Neuroscience*, *7*(8), 847–854.

Weinhard, L., di Bartolomei, G., Bolasco, G., Machado, P., Schieber, N. L., Neniskyte, U., Exiga, M., Vadisiute, A., Raggioli, A., Schertel, A., Schwab, Y., & Gross, C. T. (2018). Microglia remodel synapses by presynaptic trogocytosis and spine head filopodia induction. *Nature Communications*, *9*(1), 1228.

Wolford, E., Lahti-Pulkkinen, M., Girchenko, P., Lipsanen, J., Tuovinen, S., Lahti, J., Heinonen, K., Hämäläinen, E., Kajantie, E., & Pesonen, A.-K. (2020). Associations of antenatal glucocorticoid exposure with mental health in children. *Psychological Medicine*, *50*(2), 247–257.

Xiang, X., Piers, T. M., Wefers, B., Zhu, K., Mallach, A., Brunner, B., Kleinberger, G., Song, W., Colonna, M., Herms, J., Wurst, W., Pocock, J. M., & Haass, C. (2018). The Trem2 R47H Alzheimer's risk variant impairs splicing and reduces Trem2 mRNA and protein in mice but not in humans. *Molecular Neurodegeneration*, *13*(1), 49.

Ye, C. J., Sharpe, Z., Alemara, S., Mackenzie, S., Liu, G., Abdallah, B., Horne, S., Regan, S., & Heng, H. H. (2019). Micronuclei and genome chaos: Changing the system inheritance. *Genes (Basel)*, *10*(5), 366.

Yu, G., Wang, L. G., Han, Y., & He, Q. Y. (2012). clusterProfiler: An R package for comparing biological themes among gene clusters. *OMICS*, *16*(5), 284–287.

Zannas, A. S., Jia, M., Hafner, K., Baumert, J., Wiechmann, T., Pape, J. C., Arloth, J., Ködel, M., Martinelli, S., Roitman, M., Röh, S., Haehle, A., Emeny, R. T., Iurato, S., Carrillo-Roa, T., Lahti, J., Räikkönen, K., Eriksson, J. G., Drake, A. J., … Binder, E. B. (2019). Epigenetic upregulation of FKBP5 by aging and stress contributes to NF-κB–driven inflammation and cardiovascular risk. *Proceedings of the National Academy of Sciences*, *116*(23), 11370–11379.

Zhang, Y., Sloan, S. A., Clarke, L. E., Caneda, C., Plaza, C. A., Blumenthal, P. D., Vogel, H., Steinberg, G. K., Edwards, M. S., Li, G., Duncan, J. A., 3rd, Cheshier, S. H., Shuer, L. M., Chang, E. F., Grant, G. A., Gephart, M. G., & Barres, B. A. (2016). Purification and characterization of progenitor and mature human astrocytes reveals transcriptional and functional differences with mouse. *Neuron*, *89*(1), 37–53.

Zierhut, C., & Funabiki, H. (2020). Regulation and consequences of cGAS activation by self-DNA. *Trends in Cell Biology*, *30*(8), 594–605.

SUPPORTING INFORMATION

Additional supporting information can be found online in the Supporting Information section at the end of this article.

How to cite this article: Wei, J., Arber, C., Wray, S., Hardy, J., Piers, T. M., & Pocock, J. M. (2022). Human myeloid progenitor glucocorticoid receptor activation causes genomic instability, type 1 IFN- response pathway activation and senescence in differentiated microglia; an early life stress model. *Glia*, 1–21. https://doi.org/10.1002/glia.24325